ACS Catalysis

Research Article

pubs.acs.org/acscatalysis

Spectroscopic and Computational Study of Cr Oxide Structures and Their Anchoring Sites on ZSM-5 Zeolites

Jie Gao,[†] Yiteng Zheng,[†] Yadan Tang,[‡] Jih-Mirn Jehng,[‡,§] Robert Grybos,*[,∥] Jaroslaw Handzlik,*[,⊥] Israel E. Wachs,*[,‡] and Simon G. Podkolzin*[,†]

[†]Department of Chemical Engineering and Materials Science, Stevens Institute of Technology, Hoboken, New Jersey 07030, United States

[‡]Operando Molecular Spectroscopy & Catalysis Laboratory, Department of Chemical and Biomolecular Engineering, Lehigh University, Bethlehem, Pennsylvania 18015, United States

[§]Department of Chemical Engineering, National Chung Hsing University, Taichung, Taiwan, Republic of China

[∥]Jerzy Haber Institute of Catalysis and Surface Chemistry, Polish Academy of Sciences, Kraków 30-239, Poland

[⊥]Faculty of Chemical Engineering and Technology, Cracow University of Technology, Kraków 31-155, Poland

Supporting Information

ABSTRACT: Cr/ZSM-5 catalysts with 0.5−2.6 wt % Cr loadings and zeolites with 15−140 Si/Al ratios were characterized with in situ UV−vis, IR, and Raman spectroscopies, including operando Raman measurements under reaction conditions in methane conversion at 773−1123 K with a simultaneous online analysis of reaction products. DFT calculations with cluster and periodic models were performed with DMol^3, Gaussian 09, and VASP software packages. Isolated Cr(VI) dioxo and Cr(III) mono-oxo structures on framework Al anchoring sites were identified as the dominant species under most conditions. In the absence of gas-phase O_2 (under Ar flow) at 773 K, the Cr(VI) dioxo species on framework Al anchoring sites autoreduce, and the Cr(III) mono-oxo species remain the only observable surface Cr oxide structures. For ZSM-5 zeolites with a relatively low concentration of framework Al atoms (Si/Al ≥ 25), exposure to gas-phase O_2 at 773 K forces surface Cr oxide species to migrate from framework Al anchoring sites to Si sites on the external surface of the zeolite and form dioxo (Si−O−)$_2$Cr(=O)$_2$ and mono-oxo (Si−O−)$_4$Cr(=O) structures. The activity of Cr/ZSM-5 catalysts in methane conversion with the production of benzene and hydrogen as the main products is lower than that of Mo/ZSM-5 catalysts. The rate of benzene formation over Cr/ZSM-5 catalysts, however, is relatively stable with time on stream, in comparison to a rapidly declining rate over Mo/ZSM-5 catalysts. The zeolite-supported Cr species are highly mobile under the reaction conditions and can migrate between zeolite particles.

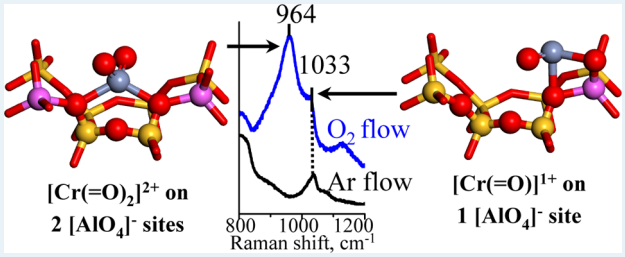

KEYWORDS: *Cr/ZSM-5, zeolite, methane dehydroaromatization, Raman spectroscopy, DFT calculations*

1. INTRODUCTION

Cr catalysts with silica and alumina supports are used in a wide range of industrial applications. For example, Cr/SiO_2 catalysts are used in the production of high-density polyethylene[1−4] and Cr/Al_2O_3 in alkane dehydrogenation.[1,3,5,6] Zeolite-supported Cr catalysts, specifically Cr/ZSM-5, have been evaluated for multiple applications, such as toluene disproportionation,[7] combustion of volatile and chlorinated organic compounds,[8−10] reduction of nitrogen oxides,[11,12] styrene selective oxidation to benzaldehyde,[13] photocatalytic partial oxidation of propane to acetone,[14] ethylene ammoxidation,[15,16] and oxidative dehydrogenation of ethane with CO_2.[17] Furthermore, Cr has been used as a promoter for other metals supported on ZSM-5 or physically mixed with ZSM-5: for example, for Mo/ZSM-5 in methane dehydroaromatization,[18] for Zn and Co/ZSM-5 in Fischer−Tropsch synthesis,[19,20] and in NO reduction by H_2.[21]

The Cr oxide structures supported on several zeolites were studied previously with diffuse reflectance spectroscopy (DRS) for multiple preparation methods and treatment conditions.[22] The catalytic performance of Cr/ZSM-5 catalysts in methane conversion was studied previously as a function of the Cr loading, zeolite acidity, and CO pretreatment.[23] The transformations of initial Cr oxide species supported on H-ZSM-5 under reaction conditions with methane were examined with X-ray photoelectron spectroscopy (XPS) measurements.[24] A recent study examined Cr oxide structures formed by incorporating Cr into the framework of an all-silica beta molecular sieve (Si-BEA) with infrared spectroscopy and density functional theory (DFT) calculations.[25] The molecular

Received: October 31, 2014
Revised: April 12, 2015
Published: April 20, 2015

DOI: 10.1021/acscatal.5b00333
ACS Catal. 2015, 5, 3078−3092

structure of Cr oxide species and their anchoring sites on ZSM-5 and other zeolites, however, remain largely unknown. Our previous studies reported experimental characterization of Cr oxide structures supported on SiO_2 and SiO_2–Al_2O_3[26−29] and computational evaluation of Cr oxide structures supported on SiO_2[30,31] as well as Mo carbide structures and their anchoring sites on ZSM-5 zeolites.[32] In this study, Mo/ZSM-5 and Cr/ZSM-5 catalysts were compared in methane dehydroaromatization, and the structure, anchoring sites, and transformations of the initial Cr oxide species for Cr/ZSM-5 catalysts with variable Cr loadings and Si/Al ratios were characterized with multiple spectroscopic techniques, including characterization under reaction conditions. DFT calculations with several zeolite models and software packages were used to analyze experimental results and identify surface Cr oxide structures and their anchoring sites on ZSM-5 zeolites.

2. EXPERIMENTAL AND COMPUTATIONAL METHODS

a. Catalyst Synthesis. Two sets of Cr/ZSM-5 catalysts were prepared by incipient wetness impregnation using aqueous chromium(III) nitrate ($Cr(NO_3)_3{\cdot}9H_2O$, Alfa Aesar, 98.5%) and H-ZSM-5 zeolites (Zeolyst International). In the first catalyst set, the Cr loading was varied between 0.5 and 2.6 wt % using an H-ZSM-5 support with the Si/Al atomic ratio of 15 (Si/Al = 15, Zeolyst CBV 3024E). In the second catalyst set, the Cr loading was kept constant at 1 wt % for H-ZSM-5 supports with different Si/Al ratios: 15 (Zeolyst CBV 3024E), 25 (Zeolyst CBV 5524G), 40 (Zeolyst CBV 8014), and 140 (Zeolyst CBV 28014). For comparison of Cr precursors, additional 0.8 wt % Cr/ZSM-5 (Si/Al = 15) catalysts were prepared with aqueous ammonium chromate ($(NH_4)_2CrO_4$, Alfa Aesar, Reagent grade). A catalyst with 1.5 wt % Mo/ZSM-5 (Si/Al = 15) was prepared with aqueous ammonium heptamolybdate ($(NH_4)_6Mo_7O_{24}{\cdot}4H_2O$, Alfa Aesar, 99.9%) using the same procedure as that for the Cr/ZSM-5 catalysts. After impregnation, the catalysts were dried at room temperature in air overnight and then by ramping to 393 K at 1 K/min and holding at this temperature for 6 h. After drying, the samples were calcined in flowing air (Airgas, ultrahigh purity) by ramping to 773 K at 1 K/min and holding at this temperature for 2 h.

b. Reaction Measurements with Methane. Reaction rate measurements were conducted in a flow system with a fixed bed reactor using a Micromeritics Autochem HP 2950 system equipped with mass flow controllers. About 0.2 g of a catalyst sample was loaded into a quartz reactor with an internal diameter of 0.44 in. The catalyst was pretreated in a flow of 10 mol % O_2/Ar (O_2, Praxair, 4.3 ultrahigh purity; Ar, Praxair, 5.0 ultrahigh purity) with a total flow rate of 100 sccm by raising the temperature at 10 K/min to 773 K and holding at this temperature for 1 h for Cr/ZSM-5 catalysts and for 2 h for Mo/ZSM-5 catalysts. After the hold in the O_2/Ar flow, the sample was purged at 773 K with Ar at 30 sccm for 30 min. The temperature was then raised to 1023 K at 10 K/min under the same Ar flow and allowed to stabilize for 15 min. Reaction measurements were performed with 10 mol % CH_4/Ar (CH_4, Praxair, 3.7 ultrahigh purity; Ar, Praxair, 5.0 ultrahigh purity) with a total flow rate of 100 sccm (GHSV = 1275 l/h) at a constant temperature of 1023 K. The testing conditions were selected in order to maintain the methane conversion below 10% for all reaction rate measurements for all Cr catalysts and, therefore, to enable use of a differential reactor model for calculating reaction rates. The methane conversion for the 1.5 wt % Mo/ZSM-5 (Si/Al = 15) catalyst declined from the initial level of ∼35% to below 10% after ∼20 min of time on stream. Reaction products were analyzed with online sampling using simultaneously a Hiden HPR-20 QIC mass spectrometer and a Varian GC-450 gas chromatograph with two thermal conductivity detector (TCD) columns (HayeSep Q 80-100 and MolSieve 5A 60-80) and one flame ionization detector (FID) column (CP8690 60 m × 0.32 mm, 5 μm, CP-Sil 5).

c. UV−vis Diffuse Reflectance Spectroscopy. Ultraviolet−visible diffuse reflectance spectroscopic (UV−vis DRS) measurements were obtained with a Varian Cary 5E UV−vis−NIR spectrophotometer employing a Harrick Praying Mantis integration sphere diffuse reflectance attachment (Model DRA-2). Samples were loaded as loose powder (∼20−35 mg) into a Harrick HVC-DR2 cell. Prior to measurements, samples were calcined and dehydrated by ramping the temperature at 1 K/min to 773 K and then holding at this temperature for 1 h under a 30 sccm flow of 10 mol % O_2/He (Airgas, certified mixture). The spectra of the dehydrated catalysts were then collected in the range of 200−800 nm under the same O_2 flow after cooling to 383 K. The reflectance of MgO was used as the baseline reference.

d. Infrared Spectroscopy. IR measurements were performed with a Thermo Scientific Nicolet 8700 Research FTIR spectrometer equipped with a liquid nitrogen cooled mercury−cadmium−telluride (MCT) detector, a Harrick Praying Mantis attachment (Model DRA-2), and a Harrick HT-100 reaction chamber. Catalyst samples (∼20 mg) were initially dehydrated in the Harrick cell under a 30 sccm flow of 10 mol % O_2/Ar (Airgas, certified mixture) by raising the temperature at 10 K/min to 773 K, holding at this temperature for 1 h, and then cooling to 383 K under the same flow for spectra acquisition. Spectra were recorded with a resolution of 4 cm^{-1} and averaged using 72 scans. IR peaks were analyzed by normalizing their areas relative to those of the Si−O−Si overtone peaks between 1730 and 2100 cm^{-1}, which were assumed to be constant for all samples.

e. Raman Spectroscopy. Raman spectra were obtained with a high-resolution, dispersive Raman spectrometer system (HORIBA LabRam HR) equipped with three laser excitations (532, 442, and 325 nm). In this study, the laser excitation of 442 nm (violet) was used with a power of 28 mW at the sample. The laser was focused on a sample with a confocal microscope equipped with a 50× long working distance Olympus BX-30-LWD objective. The LabRam HR spectrometer was optimized for the best spectral resolution by employing a 900 grooves/mm grating (HORIBA 51093140HR), giving a typical spectral resolution of ∼2 cm^{-1}. The calibration laser line was measured by an Hg lamp for the zero position and linearity of the gratings. The wavenumber calibration of the Raman spectrograph was checked using the silicon line at 520.7 cm^{-1}. The Rayleigh scattered light was rejected with holographic notch filters (Kaiser Super Notch) containing window cutoffs of ∼100 cm^{-1}. A catalyst sample (5−10 mg of loose powder) was placed in a high-temperature flow reactor (Linkam CCR1000) with a quartz window and O-ring seals, which were cooled by flowing water. The sample temperature was controlled by a Linkam LinkPad temperature controller.

In situ Raman spectra under oxygen flow were collected by first dehydrating a catalyst sample in a flow reactor by ramping the temperature at 10 K/min to 773 K and holding at this temperature for 1 h under a 30 sccm flow of 10 mol % O_2/Ar

DOI: 10.1021/acscatal.5b00333
ACS Catal. 2015, 5, 3078−3092

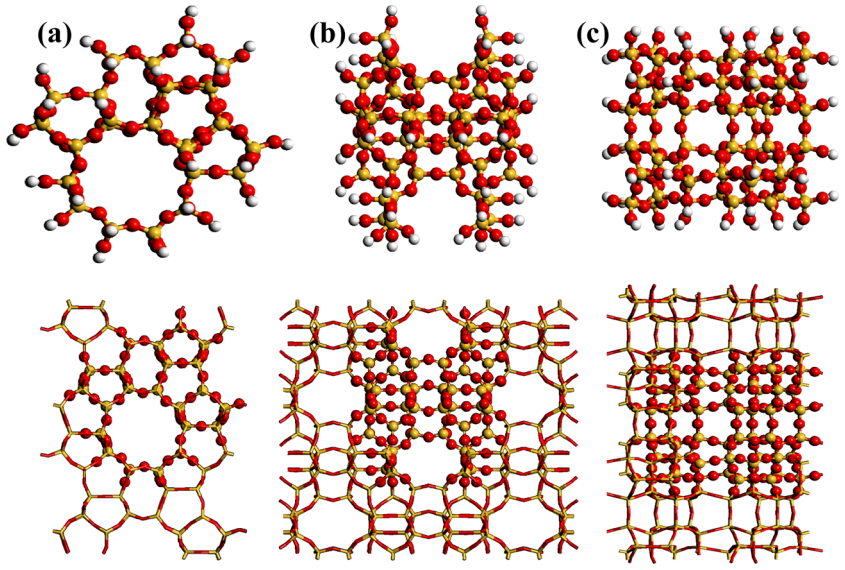

Figure 1. 64-T cluster model of the ZSM-5 structure (ball and stick representation) shown separately in the top row and shown in the ZSM-5 unit cell (wire frame representation) in the bottom row: (a) channel view; (b) side view; (c) top view. This model was used in DMol^3 DFT calculations.

(Airgas, certified mixture). After this dehydration pretreatment, Raman spectra were collected under the same O_2/Ar flow at 773 K at a scanning rate of 25 s/scan and a total of 30 scans with a 200 μm hole, at which only laser angles parallel to the incident beam were acquired from the light scattered by the catalyst sample. After the spectra acquisition at 773 K, the temperature was decreased to 383 K under the O_2/Ar flow, and additional Raman spectra were collected at this lower temperature.

Operando Raman spectra under reaction conditions with methane, simultaneous spectroscopic monitoring of the catalyst and online mass spectrometry analysis of products, were collected for a 0.5 wt % Cr/ZSM-5 (Si/Al = 15) catalyst. For these measurements, a sample (20−35 mg) was first pretreated in a Linkam 9754 CCR-B reactor cell by raising the temperature with a ramp rate of 10 K/min to 773 K under a 30 sccm flow of 10 mol % O_2/Ar (Airgas, certified mixture) and holding at this temperature under the same flow for 1 h. The cell was then flushed with a 30 sccm Ar flow (Airgas, ultrahigh purity) for 30 min. After the flush, a flow of 1.5 mol % CH_4/He (Airgas, high purity) was introduced at a total flow rate of 30 sccm, and the temperature was increased at a ramp rate of 1 K/min from 773 to 1123 K. Raman spectra were collected continuously at 30 s/scan, and reaction products were continuously analyzed with online mass spectrometry measurements at 0.5 s/scan.

f. DFT Models and Computational Settings. *f-1. Cluster Calculations with DMol^3 in Materials Studio.* Gradient-corrected DFT calculations were performed with the DMol^3 code in Materials Studio 4.0 program by BIOVIA Corp. The calculations used the DNP basis set and the GGA RPBE functional. Tightly bound core electrons for Cr were represented with semicore pseudopotentials. Reciprocal-space integration over the Brillouin zone was approximated through Γ-point sampling (1 × 1 × 1 Monkhorst−Pack grid). The density mixing fraction of 0.2 with direct inversion in the iterative subspace (DIIS) and orbital occupancy with smearing of 0.005 Ha were used. The orbital cutoff distance was set at 0.44 nm for all atoms.

The ZSM-5 structure was modeled with a 64-T cluster ($Si_{64}O_{155}H_{54}$), shown in Figure 1. The cluster was generated from two adjacent MFI unit cells (96 × 2 = 192 Si atoms and 192 × 2 = 384 O atoms) with the initial lattice constants of a = 2.0022 nm, b = 1.9899 nm, and c = 1.3383 nm. The dangling bonds of the boundary O atoms in the cluster were saturated by H atoms. In order to minimize cluster boundary effects and better simulate the overall zeolite structure, the coordinates of these terminal OH groups were constrained. The terminal O atoms were constrained at their original positions in the MFI unit cell. The terminal H atoms were constrained at the positions obtained with the following two-step procedure. First, the bonding Si atoms from the part of the zeolite framework that was cut out from the cluster were changed into H atoms. Second, the distance between the bonding O atoms in the cluster and the terminal H atoms was adjusted to 0.095 nm. Except for the terminal OH groups, all other atoms were optimized with Cr oxide structures. Normal vibrational modes were calculated with a partial Hessian matrix for Cr oxide structures. Calculated frequencies were adjusted with a scaling factor of 0.9583.

f-2. Periodic Unit Cell Calculations with VASP. Spin-polarized DFT calculations with the full periodic ZSM-5 unit cell (96 Si and 192 O atoms) were performed with the PW91 functional[33] using the VASP code.[34,35] Valence electrons were described using plane waves with a cutoff energy of 400 eV. Tightly bound core electrons were represented with PAW pseudopotentials.[36] Positions of all atoms were optimized without changing the initial lattice constants of a = 2.007 nm, b = 1.992 nm, and c = 1.342 nm.[37]

Normal vibrational modes were calculated using a harmonic approximation with a partial Hessian matrix for Cr oxide structures. Additional calculations showed that changes in vibrational frequencies are within 3 cm^{-1} when the atoms in the zeolite ring of the anchoring site are included in the Hessian matrix. Calculated frequencies were adjusted with a scaling factor of 0.9339 on the basis of a least-squares fit for Cr═O experimental vibrational frequencies in reference compounds: $CrOF_4$, CrO_2F_2, CrO_2Cl_2, $CrO(OH)_2$, $HCrO(OH)$, and $CrO(OH)$.[38−40]

DOI: 10.1021/acscatal.5b00333
ACS Catal. 2015, 5, 3078−3092

f-3. Cluster Calculations with Gaussian 09. Geometry optimization DFT calculations were performed using the PW91 functional with the split-valence def2-SVP basis set[41] using the Gaussian 09 software package.[42] After geometry optimization, single-point energy calculations were performed with the PW91 functional and the triple-ζ valence def2-TZVPP basis set.[41] Spin-restricted calculations were used for closed-shell systems with Cr(VI) oxide species.

The ZSM-5 structure was modeled with two separate 46-T clusters ($Si_{46}O_{111}H_{38}$). One cluster is shown in Figure 2, and

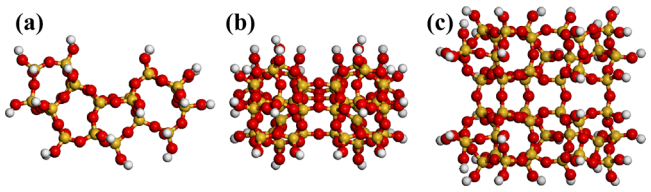

Figure 2. 46-T cluster model of the ZSM-5 zeolite structure: (a) channel view; (b) side view; (c) top view. This model was used in Gaussian 09 DFT calculations.

the second similar cluster, which represents a different ZSM-5 fragment, is shown in Figure S1 in the Supporting Information. Both clusters were generated from an MFI unit cell, in which the positions of all atoms had been previously optimized with the VASP periodic calculations. The dangling bonds of the boundary O atoms in the clusters were saturated by H atoms. In order to minimize cluster boundary effects and better simulate the overall zeolite structure, the coordinates of these terminal OH groups were constrained. The terminal O atoms were constrained at their original positions in the optimized MFI unit cell. H atoms were placed at a distance of 0.097 nm from O atoms along the O−Si bond directions of the optimized ZSM-5 structure. Normal vibrational modes were calculated with the full Hessian matrix. Calculated frequencies were adjusted with a scaling factor of 0.9149.[30]

3. RESULTS

a. Reaction Measurements with Methane. Mass spectrometry (MS) results for reaction products as a function of time on stream with methane at 1023 K for 0.8 wt % Cr/ZSM-5 (Si/Al = 15) are shown in Figure 3 for two runs. In the first run, the catalyst was tested after calcination in air (Figure 3a). In the second run, the catalyst was pretreated after calcination, and prior to testing with methane, under a 10 mol % O_2 flow at 773 K for 1 h followed by an Ar purge at the same temperature for 30 min (Figure 3b). After this O_2 flow treatment with the Ar purge, the color of the catalyst changed from pale yellow, indicating the presence of Cr(VI) cations, to pale green, indicating the presence of Cr(III) cations. Photos of the catalysts are included in Figure 3. In both runs, once methane is introduced into the reactor (time on stream of 0), formation of H_2, C_2H_4, H_2O, CO_2, and C_6H_6 (benzene) is observed almost immediately. Formation of H_2O and CO_2 indicates reduction of Cr oxide species. The reduction process under these testing conditions is complete after 4 min of time on stream when the signal for CO_2 decreases to the baseline level. Evolution of produced H_2O continues for an extended period of time, since the zeolite support retains moisture. The amount of produced CO_2 for the catalyst after the O_2 pretreatment with the Ar purge (Figure 3b) is actually lower than that for the catalyst without the pretreatment (Figure 3a),

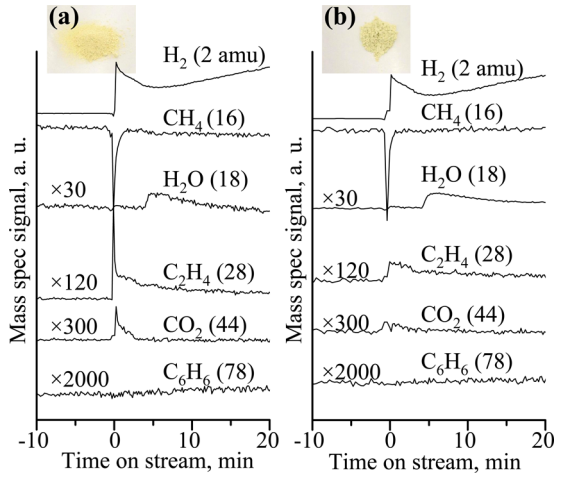

Figure 3. Evolution of reaction products in methane conversion over 0.8 wt % Cr/ZSM-5 (Si/Al = 15) catalyst: (a) after calcination; (b) after calcination followed by dehydration under 10 mol % O_2/Ar and then Ar flows at 773 K. The photos show the catalysts before reaction testing. Reaction conditions: 100 sccm flow of 10 mol % CH_4/Ar, 0.2 g of catalyst, 1023 K.

suggesting that such a pretreatment partially reduces Cr oxide species. The detection of benzene and hydrogen formation almost immediately after methane introduction, simultaneously with CO_2 and H_2O evolution, in Figure 3 signifies that the Cr/ZSM-5 samples catalyze methane dehydroaromatization with the main reaction $6CH_4 = C_6H_6 + 9H_2$ even before the completion of the initial period when Cr oxide species are reduced.

Changes in benzene and hydrogen formation rates as a function of time on stream on a longer time scale were evaluated with gas chromatography (GC) measurements under the same testing conditions at 1023 K. The reaction rates in Figure 4 compare turnover frequencies (TOF: moles of C_6H_6 or H_2 produced per mole of catalytic metal per second) for 0.8 wt % Cr/ZSM-5 (Si/Al = 15) and 1.5 wt % Mo/ZSM-5 (Si/Al = 15) catalysts. The loading of the Mo catalyst in moles of Mo

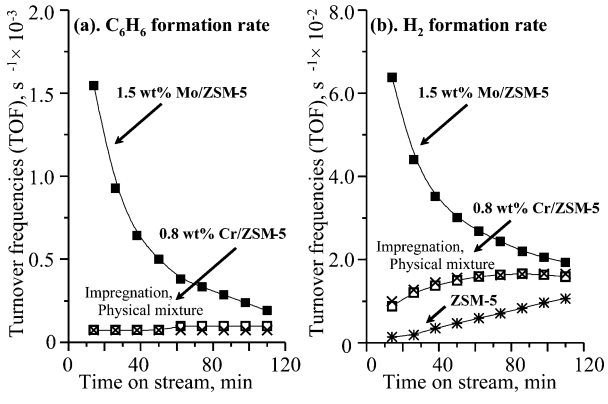

Figure 4. Formation rates of (a) benzene and (b) hydrogen over 0.8 wt % Cr and 1.5 wt % Mo (same number of moles) supported on ZSM-5 (Si/Al = 15) in catalytic methane dehydroaromatization with the main reaction $6CH_4 = C_6H_6 + 9H_2$. Reaction conditions: 100 sccm flow of 10 mol % CH_4/Ar, 0.2 g of catalyst, 1023 K. Legend: (■) 1.5 wt % Mo/ZSM-5; (□) 0.8 wt % Cr/ZSM-5 prepared by impregnation; (×) 0.8 wt % Cr/ZSM-5 as a 1:1 physical mixture of 1.6 wt % Cr/ZSM-5 and ZSM-5; (∗) ZSM-5 without metals.

DOI: 10.1021/acscatal.5b00333
ACS Catal. 2015, 5, 3078−3092

per unit mass matches the metal loading of the Cr catalyst. The formation rates for both benzene and hydrogen over the Mo/ZSM-5 catalyst decline rapidly with time on stream. The 0.8 wt % Cr/ZSM-5 catalyst exhibits a significantly lower activity than Mo/ZSM-5, but the rate of benzene formation is relatively stable. The rate of hydrogen formation for the 0.8 wt % Cr/ZSM-5 catalyst actually increases with time on stream, signifying a progressively lower selectivity to benzene.

When the Cr concentration is doubled to 1.6 wt % using the same ZSM-5 (Si/Al = 15) support, the catalytic performance remains largely unchanged. Therefore, the rates of hydrogen and benzene formation per Cr atom are lower than those for the 0.8 wt % Cr/ZSM-5 catalyst by about a factor of 2 (Figure S2 in the Supporting Information).

The zeolite support without metals, H-ZSM-5 (Si/Al = 15), exhibits a small but measurable activity in methane activation. This is illustrated in Figure 4b as turnover frequencies for H_2 formation calculated analogously to those for the 0.8 wt % Cr and 1.5 wt % Mo/ZSM-5 samples with the same amount of ZSM-5. The rate of hydrogen formation is initially negligibly small and then increases with time on stream, possibly due to the formation of carbonaceous surface deposits that can catalyze methane decomposition. The amount of produced benzene, however, remains at or below the detection limit for the whole duration of the run, and the corresponding negligibly small benzene formation rates for the blank H-ZSM-5 are not shown in Figure 4a.

The reaction measurement results shown in Figure 4 are similar for 0.8 wt % Cr/ZSM-5 catalysts prepared with two different Cr precursors: chromium nitrate ($Cr(NO_3)_3{\cdot}9H_2O$) and ammonium chromate ($(NH_4)_2CrO_4$). The similarity in catalytic performance suggests that the initially different Cr species in the precursors as a cation and an anion convert into the same zeolite-supported Cr oxide species during the catalyst pretreatment in the presence of gas-phase oxygen at elevated temperatures. In order to further probe the nature of the zeolite-supported Cr oxide species, an additional Cr/ZSM-5 formulation was prepared as a 1:1 by weight physical mixture of H-ZSM-5 (Si/Al = 15) and 1.6 wt % Cr/ZSM-5 (Si/Al = 15), producing a sample with the overall nominal formulation equivalent to 0.8 wt % Cr/ZSM-5. The results in Figure 4 demonstrate that the hydrogen and benzene formation rates are the same within the experimental accuracy for this physical mixture and for the 0.8 wt % Cr/ZSM-5 catalyst prepared by impregnation. The Cr species, therefore, must be highly mobile under the pretreatment or reaction conditions, as they migrate in the physical mixture from the impregnated part of the sample to the blank H-ZSM-5. If such a migration of Cr species did not take place, the performance of the physical mixture would be a simple sum of activities of its parts with lower benzene formation rates and selectivities due to the significantly lower performance of the blank H-ZSM-5.

b. In Situ UV−vis Diffuse Reflectance Spectroscopy. The nature of Cr oxide species and their anchoring sites for 0.5 wt % Cr/ZSM-5 (Si/Al = 15, 25, 40, 140) catalysts under a 10 mol % O_2 flow at 383 K were evaluated with in situ UV−vis DRS measurements. The UV−vis DRS spectra shown in Figure 5 exhibit several ligand-to-metal charge-transfer (LMCT) transitions. For the Cr/ZSM-5 samples with high Al concentrations (Si/Al = 15, 25), two prominent LMCT transitions are observed at 252 and 324 nm. These spectral features match the LMCT transitions (~250 and ~350 nm) for isolated Cr oxide species anchored on exposed alumina sites in

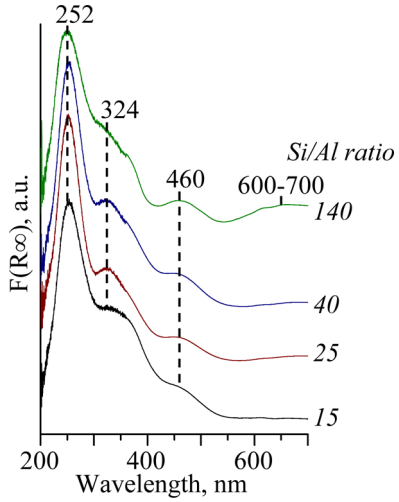

Figure 5. In situ UV−vis DRS spectra for 1.0 wt % Cr supported on ZSM-5 zeolites with variable Si/Al ratios collected at 383 K under 10 mol % O_2/He after dehydration at 773 K for 1 h.

dehydrated Al_2O_3/SiO_2 supports.[1,29] At a lower Al concentration (Si/Al = 40), the LMCT band at 460 nm becomes more prominent in addition to the LMCT transitions at 252 and 324 nm. This band is indicative of isolated Cr oxide species anchored on silica sites, representing the LMCT of the O(2p) to Cr(d) orbital.[1,26] At the lowest Al concentration (Si/Al = 140), a new additional d−d LMCT transition is observed at ~600 nm. This new UV−vis transition falls in the range of crystalline Cr_2O_3 nanoparticles.[1,26] The silica-rich Cr/ZSM-5 (Si/Al = 140) sample, thus, contains isolated Cr oxide species as well as crystalline Cr_2O_3 nanoparticles.

The in situ UV−vis spectra demonstrate that isolated Cr oxide species anchored on Al sites are dominant in dehydrated Cr/ZSM-5 catalysts for the alumina-rich ZSM-5 supports (Si/Al = 15 and 25) at 383 K. As the Al concentration in the zeolite support decreases, surface Cr oxide species increasingly anchor on Si sites. Crystalline Cr_2O_3 nanoparticles are also observed on the surface of the silica-rich ZSM-5 support (Si/Al = 140) when the concentration of Al anchoring sites is very low.

c. In Situ Infrared Spectroscopy. The anchoring sites of Cr oxide species on the ZSM-5 (Si/Al = 15) zeolite as a function of the Cr loading were evaluated under a 10 mol % O_2 flow at 383 K with in situ IR measurements. The IR spectra in Figure 6 provide information on vibrations of OH groups on the surface of the initial H-ZSM-5 support and on changes in these surface OH groups caused by the presence of Cr oxide species for 0.5, 1.0, and 1.6 wt % Cr loadings. The IR spectra in the OH vibrational region in Figure 6 exhibit two main peaks at 3608 and 3741 cm^{-1} and two smaller peaks at 3783 and 3660 cm^{-1}. These peaks correspond to different types of surface OH groups. The peak at 3608 cm^{-1} is due to vibrations of Brønsted acid hydroxyls on zeolite framework Al sites. The peak at 3741 cm^{-1} is due to vibrations of silanol Si−OH groups on the external surface of the zeolite. Finally, the peaks at 3783 and 3660 cm^{-1} are due to vibrations of OH groups on extraframework Al sites. Similar IR peaks were analyzed in our previous study of anchoring sites for Mo oxide species on ZSM-5 zeolites.[32] The intensity of the peak at 3741 cm^{-1} from Si−OH groups steadily decreases with increasing Cr loading, reflecting anchoring of Cr oxide species on Si sites on the external surface of the zeolite. The intensities of the IR peaks at

DOI: 10.1021/acscatal.5b00333
ACS Catal. 2015, 5, 3078−3092

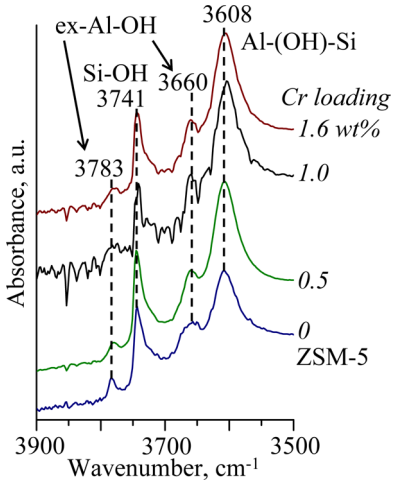

Figure 6. In situ IR spectra for Cr/ZSM-5 catalysts as a function of the Cr loading. Spectra were collected at 383 K under 10 mol % O_2/He after dehydration at 773 K for 1 h.

3783 and 3660 cm^{-1} from OH groups on extraframework Al sites do not change appreciably. This suggests that Cr oxide species do not anchor on these sites or that anchoring of a small fraction of Cr oxide species is offset by some zeolite dealumination (migration of Al atoms from framework to extraframework positions). The intensity of the IR peak at 3608 cm^{-1} from OH groups on framework Al sites actually increases with the introduction of Cr oxide species. Such an increase can be rationalized by anchoring of Cr oxide species with an OH group, for example $[Cr(=O)_2OH]^+$, on framework $[AlO_4]^-$ sites if the vibration of the OH group bonded to the Cr atom remains at ~3608 cm^{-1} and the IR extinction coefficient for this vibration is higher than that for the original OH on the Al framework site. Formation of Cr oxide species with multiple OH groups is unlikely after our dehydration pretreatment at 773 K. The observed trends in IR spectra, therefore, suggest that Cr oxide species anchor on Si sites on the external surface of the zeolite. In addition, anchoring on extraframework Al sites is likely minimal and, finally, anchoring on framework Al sites should involve some Cr oxide species with OH groups.

d. In Situ and Operando Raman Spectroscopy. The vibrations of the surface Cr oxide structures were examined with in situ Raman spectroscopy. Spectra were collected under a 10 mol % O_2 flow at 383 K (Figure 7a,b) and at 773 K (Figure 7c). At the lowest Cr loading of 0.5 wt % on the dehydrated ZSM-5 (Si/Al = 15) zeolite at 383 K, two main bands are present at 964 and 1033 cm^{-1} (Figure 7a). These Raman bands remain dominant as the Cr loading increases to 2.6 wt %. In addition, a smaller band at 1017 cm^{-1} becomes progressively larger with increasing Cr loading for the same ZSM-5 (Si/Al = 15) support. This smaller band is similar to the Raman band at ~1010 cm^{-1} reported in our previous studies for CrO_x/SiO_2 catalysts.[26,29] Therefore, it is likely that the band at 1017 cm^{-1} is due to Cr oxide species anchored on Si zeolite sites, and the bands at 964 and 1033 cm^{-1}, which are not observed in the Raman spectra for CrO_x/SiO_2, are due to Cr oxide species anchored on Al zeolite sites.

The in situ Raman spectra for the dehydrated 1 wt % Cr/ZSM-5 catalyst at 383 K for zeolites with Si/Al ratios from 15 to 140 are shown in Figure 7b. The spectrum for 1 wt % Cr/ZSM-5 (Si/Al = 15) is shown in both Figure 7a (effect of the Cr loading) and Figure 7b (effect of the Si/Al ratio) for comparison. As mentioned above, this Raman spectrum exhibits two main bands at 964 and 1033 cm^{-1}. As the Si/Al ratio increases from 15 to 25 and then to 40 (Figure 7b), the Raman band at 1033 cm^{-1} is no longer observed and, instead, the band at 1017 cm^{-1} is detected. These changes demonstrate that the initial bands at 964 and 1033 cm^{-1} must be from two different Cr oxide species anchored on Al zeolite sites, because the intensities of these two bands are not correlated. The Raman spectra also show that Cr oxide species preferentially anchor on Al zeolite sites (Raman bands at 964 and 1033 cm^{-1}). As the concentration of Al sites decreases with the increasing Si/Al ratio, Cr oxide species begin to anchor on Si sites (Raman band at 1017 cm^{-1}). At the highest Si/Al ratio of 140 (lowest Al concentration), Raman bands at 964 and 1033 cm^{-1} for Cr oxide species on Al sites are not observed at all (Figure 7b). Instead, the spectrum for 1 wt % Cr/ZSM-5 (Si/Al = 140) exhibits bands at 984 and 1017 cm^{-1}, which must be from Cr oxide species anchored on Si sites. These bands are, indeed, similar to the bands at ~978 and ~1010 cm^{-1} reported in our previous studies for CrO_x/SiO_2.[26,29]

The Raman spectra in Figure 7c were collected at a higher temperature of 773 K for the same 1 wt % Cr/ZSM-5 (Si/Al = 25, 40, and 140) catalysts as those shown in Figure 7b (spectra at 383 K). All spectra at this higher temperature exhibit bands at 984 and 1017 cm^{-1} for Cr oxide species anchored on Si sites. In contrast with the spectra in Figure 7b, the bands at 964 and 1033 cm^{-1} for Cr oxide species anchored on Al sites are not observed at all at this higher temperature. These results, therefore, suggest that Cr oxide species are highly mobile on

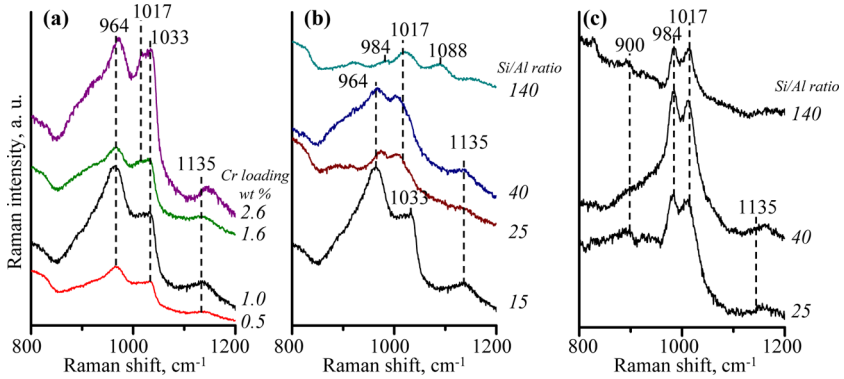

Figure 7. In situ Raman spectra (442 nm) for Cr/ZSM-5 catalysts under 10 mol % O_2/Ar flow: (a) as a function of the Cr loading for ZSM-5 (Si/Al = 15) at 383 K; (b) as a function of the Si/Al ratio for 1 wt % Cr at 383 K; (c) same as (b) but spectra collected at 773 K.

DOI: 10.1021/acscatal.5b00333
ACS Catal. 2015, 5, 3078−3092

the surface of ZSM-5 zeolites and that an exposure to gas-phase O_2 at elevated temperatures forces Cr oxide species to migrate from Al to Si anchoring sites.

An additional experiment was performed in order to confirm that the Raman bands at 964 and 1033 cm^{-1} assigned to Cr oxide species anchored on Al sites are indeed due to two different structures and are not due to the symmetric and asymmetric stretches (ν_s and ν_{as}) of a single Cr oxide structure. After a Raman spectrum was collected for the 0.5 wt % Cr/ZSM-5 (Si/Al = 15) sample at 773 K under a 10 mol % O_2 flow, the flow was switched to Ar. Figure 8 compares the

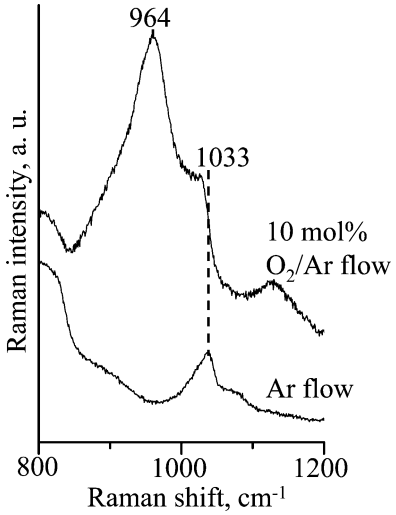

Figure 8. In situ Raman spectra (442 nm) for the 0.5 wt % Cr/ZSM-5 (Si/Al = 15) catalyst at 773 K after pretreatment under 10 mol % O_2/Ar at 773 K for 1 h. In the experiment, the flow was switched from 10 mol % O_2/Ar to Ar.

spectra collected under O_2 and Ar flows. The spectrum in the presence of gas-phase O_2 exhibits both bands at 964 and 1033 cm^{-1}. In contrast, in the absence of gas-phase O_2, the band at 964 cm^{-1} is no longer observed due to preferential reduction. This observation confirms that the bands at 964 and 1033 cm^{-1} are indeed from two different surface Cr oxide species and shows that the surface Cr oxide species associated with the band at 964 cm^{-1} autoreduce in Ar at 773 K. The spectra in Figure 8 also demonstrate that, when there is a sufficient number of Al framework anchoring sites (Si/Al = 15) and the Cr loading is relatively low (0.5 wt %), Cr oxide species preferentially anchor on framework Al sites and exposure to gas-phase O_2 at 773 K does not force a migration of surface Cr oxide species to Si sites, as observed for the 1 wt % Cr/ZSM-5 samples with Si/Al ratios of 25, 40, and 140 in Figure 7c.

Some of the spectra in Figures 7 and 8 exhibit a broad feature at ~1135 cm^{-1}. The disappearance of this feature under the Ar flow in Figure 8 shows that it is from surface Cr oxide species rather than from the zeolite support. This feature is possibly due to Cr oxide species anchored on extraframework Al sites.

The transformation of Cr oxide species under reaction conditions with methane was monitored with operando Raman spectroscopy with simultaneous analysis of reaction products with online MS measurements, and the results for the 0.5 wt % Cr/ZSM-5 (Si/Al = 15) catalyst are presented in Figure 9. The first Raman spectrum in Figure 9a was collected at 773 K under an Ar flow prior to methane introduction (time on stream of 0). It exhibits a single band at 1033 cm^{-1} for Cr oxide species

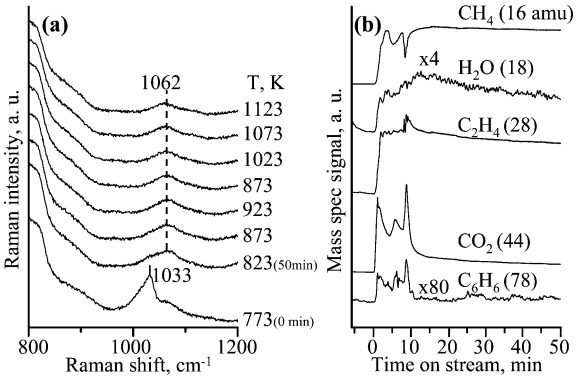

Figure 9. (a) Operando Raman spectra (442 nm) and (b) corresponding mass spectra for methane conversion over the 0.5 wt % Cr/ZSM-5 (Si/Al = 15) catalyst. Reaction conditions: 1.5 mol % CH_4/Ar flow, temperature increased linearly from 773 K at 1 K/min.

anchored on framework Al sites. This spectrum with a single band at 1033 cm^{-1} is similar to the spectrum in Figure 8 collected for the same catalyst under similar conditions after switching the flow from O_2 to Ar. After the feed was switched to a 1.5 mol % CH_4/He flow, the reactor temperature was increased at a rate of 1 K/min. After 50 min of time on stream at 823 K, the band at 1033 cm^{-1} for Cr oxide species is no longer observed, and a new band appears at 1062 cm^{-1} characteristic of polycyclic aromatic hydrocarbons on zeolite surfaces. The spectra remain unchanged with a single band at 1062 cm^{-1} until the completion of the experiment at 1123 K in 350 min (Figure 9a). Figure 9b shows MS spectra for the reaction products obtained simultaneously with the operando Raman spectra in Figure 9a. These MS spectra collected at a constant temperature ramp rate starting at 773 K are qualitatively similar to the MS spectra in Figure 3 obtained at a constant temperature of 1023 K. The spectra show that during the initial reaction period some Cr oxide species are reduced, as evidenced by the formation of CO_2 and H_2O.

e. DFT Calculations. Multiple Cr oxide species on different zeolite anchoring sites were evaluated with DFT calculations with the objective of identifying structures that have normal vibrational modes that match the experimentally observed Raman bands and are also consistent with other characterization and testing results.

Since the in situ UV−vis spectra in Figure 5 suggest that the surface Cr oxide species are isolated, only structures with a single Cr atom were evaluated with DFT calculations. After exposure to gas-phase O_2 at elevated temperatures, surface Cr is expected to be in its highest oxidation state of +6.[1,22,24] Furthermore, the in situ Raman spectra in Figure 8 demonstrate that zeolite-supported Cr oxide species can autoreduce under Ar in the absence of gas-phase O_2. Therefore, other oxidation states were also evaluated.

The in situ UV−vis spectra in Figure 5 and the in situ IR spectra in Figure 6 suggest that the Cr oxide species anchor on the following sites: framework Al sites, extraframework Al sites, and Si sites on the external surface of the ZSM-5 zeolite. Framework Al sites and Si sites on the external surface of the zeolite were evaluated. In addition, defect zeolite sites caused by a Si or Al atom vacancy were evaluated. Extraframework Al sites were not evaluated in this study, since only a small fraction of Cr oxide species is expected to anchor on these sites.

The computational results for Cr oxide species anchored on framework Al sites are summarized in Table 1. If two Al atoms

DOI: 10.1021/acscatal.5b00333
ACS Catal. 2015, 5, 3078−3092

Table 1. Vibrational Modes (Symmetric Stretch ν_s, Asymmetric Stretch ν_{as}, and Bend δ) of Cr Oxide Species Anchored on Framework Al Sites[a]

(a) Dioxo Cr Species				
	Cr oxidation state	ν_s(O═Cr═O), cm^{-1}	ν_{as} (O═Cr═O), cm^{-1}	δ(O═Cr═O), cm^{-1}
$[Cr(=O)_2]^{2+}$ on 2 $[AlO_4]^-$	+6	964–970 (919–986)[b] (973–994)[c]	971–1000 (1010–1026)[b] (1017–1033)[c]	392–430 (379–462)[b]
$[Cr(=O)_2OH]^+$ on 1 $[AlO_4]^-$	+6	956–971	993–1011	391–418
$[Cr(=O)_2]^+$ on 1 $[AlO_4]^-$	+5	937–957	966–988	407–424
experimental Raman band in Figures 7 and 8		964		
(b) Mono-oxo Cr Species				
		Cr oxidation state	ν(Cr═O), cm^{-1}	
$[Cr(=O)]^{2+}$ on 2 $[AlO_4]^-$		+4	1017–1048	
$[Cr(=O)]^+$ on 1 $[AlO_4]^-$		+3	1025–1038	
experimental Raman band in Figures 7–9			1033	

[a]Results obtained with DFT calculations with DMol^3 using a 64-T cluster zeolite model. [b]Additional results obtained with Gaussian 09 using a 46-T cluster zeolite model. [c]Additional results obtained with VASP using a full periodic unit cell.

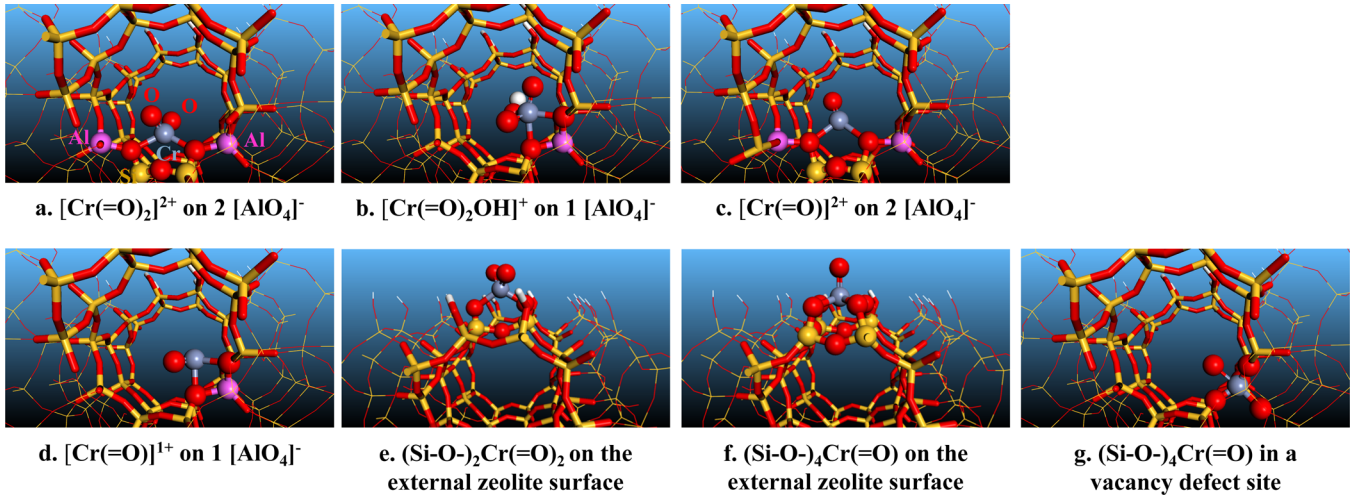

Figure 10. Structures of isolated Cr oxide species anchored on ZSM-5 sites obtained with DMol^3 DFT calculations.

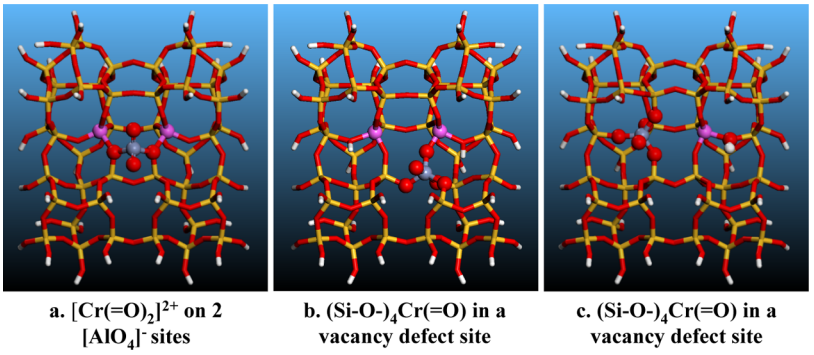

Figure 11. Structures of isolated Cr oxide species anchored on ZSM-5 sites obtained with Gaussian 09 DFT calculations.

are in proximity in the zeolite framework, they can serve as a single anchoring site by bridge-bonding Cr oxide species. Such a geometry for dioxo $[Cr(=O)_2]^{2+}$ species obtained with the 64-T ZSM-5 model (Figure 1) using the DMol^3 DFT code is shown in Figure 10a for a pair of Al atoms in T8–T12 sites. In this dioxo structure, the Cr atom is terminated with two oxygen atoms and is bridge-bonded to the zeolite through two framework oxygen atoms adjacent to the Al atoms. The dioxo $[Cr(=O)_2]^{2+}$ structure anchored on two framework $[AlO_4]^-$ sites was evaluated for Al atoms in the following T site pairs: T3–T3, T4–T12, T7–T12, and T8–T12. The calculated normal vibrational modes for the symmetric stretch (ν_s) for the dioxo $[Cr(=O)_2]^{2+}$ species anchored on these sites are similar, in the range of 964–970 cm^{-1} (Table 1a).

Similar structures with similar vibrational modes were obtained with the 46-T ZSM-5 models (Figure 2 and Figure S1 in the Supporting Information) using Gaussian 09 calculations for anchoring Al atoms in T7–T10 and T8–T8

DOI: 10.1021/acscatal.5b00333
ACS Catal. 2015, 5, 3078–3092

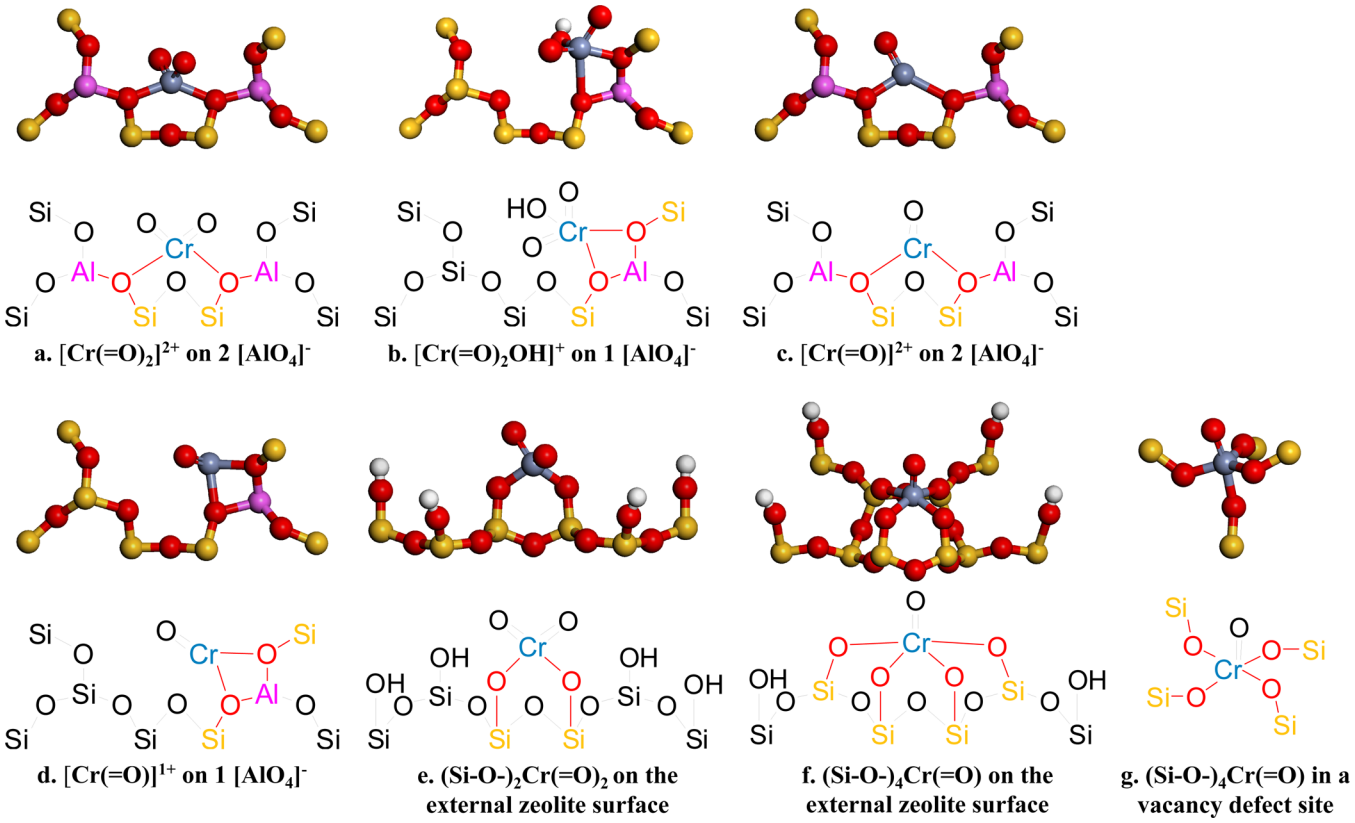

Figure 12. Schematic representations of zeolite-anchored Cr oxide structures shown in Figure 10

sites. The dioxo $[Cr(=O)_2]^{2+}$ structure anchored on a pair of Al atoms in T8−T8 sites with calculated ν_s 982 cm^{-1} (Table 1a) is shown in Figure 11a, and a similar structure for T7−T10 sites is shown in Figure S3a in the Supporting Information (ν_s 919 cm^{-1} and another symmetric stretch mode coupled with support vibrations at 986 cm^{-1}). The molecular structure and vibrational modes were further examined with the full periodic ZSM-5 unit cell calculations using the VASP software package for Al atoms in the same T7−T10 and T8−T8 sites. The obtained geometries shown in Figure S4a,b in the Supporting Information and the range for the symmetric stretching mode ν_s 973−994 cm^{-1} (Table 1a) are consistent with those obtained using the cluster models.

Schematic representations for the dioxo $[Cr(=O)_2]^{2+}$ species anchored on a pair of framework Al atoms and other evaluated surface Cr oxide structures are provided in Figure 12. If a framework Al atom does not have another framework Al atom in proximity, it can serve as a single Al-atom anchoring site. In order for Cr dioxo species to anchor on such a site and maintain the Cr atom in its highest oxidation state of +6, the Cr structure should include an OH group. A representative optimized structure of $[Cr(=O)_2OH]^{+}$ species anchored on 1 $[AlO_4]^{-}$ site in a T12 position is shown in Figure 10b and schematically in Figure 12b. This structure with the Cr atom bridge-bonded to a framework Al atom through neighboring framework O atoms as O−Al−O is more stable than similar structures bonded simultaneously to Al and Si framework atoms as O−Si−O−Al. The dioxo $[Cr(=O)_2OH]^{+}$ structure anchored on one framework $[AlO_4]^{-}$ site was evaluated for an Al atom in the following T sites: T3, T5, T8, T11, and T12. The obtained ν_s values are in the range 956−971 cm^{-1}, which is similar to the 964−970 cm^{-1} range for the dioxo $[Cr(=O)_2]^{2+}$ species anchored on two $[AlO_4]^{-}$ sites (Table 1a). These frequencies match the experimental Raman band at 964 cm^{-1} in Figures 7 and 8.

If the structure of Cr dioxo species on a single Al-atom framework anchoring site does not include an OH group, the formal oxidation state of Cr changes to +5, which is usually less stable than +6 or +3 oxidation states. Since a trace presence of Cr(V) oxide species was detected with electron spin resonance spectroscopy (ESR) for $Cr/SiO_2-Al_2O_3$ catalysts,[1,43,44] a Cr(V) structure as a $[Cr(=O)_2]^{+}$ species anchored on one $[AlO_4]^{-}$ site was evaluated for an Al atom in the following T sites: T3, T4, T5, T7, and T8. The obtained ν_s values in the range 937−957 cm^{-1} do not match positions of the experimental Raman bands (Table 1a).

Cr mono-oxo species may anchor on both single and double Al-atom framework sites. The structure of mono-oxo $[Cr(=O)]^{2+}$ species anchored on two $[AlO_4]^{-}$ sites with the Cr oxidation state of +4 was evaluated for Al atoms in the following T site pairs: T4−T4, T8−T12, and T11−T11. A representative $[Cr(=O)]^{2+}$ structure anchored on a pair of Al atoms in T8−T12 sites with ν 1023 cm^{-1} is shown in Figure 10c. In this structure, the Cr atom is terminated by a single O atom and is bridge-bonded to the zeolite through two framework O atoms adjacent to the Al atoms. A similar mono-oxo $[Cr(=O)]^{+}$ structure anchored on one $[AlO_4]^{-}$ site instead of two $[AlO_4]^{-}$ sites produces Cr(III) mono-oxo species. Anchoring of these $[Cr(=O)]^{+}$ species was evaluated for an Al atom in T3, T7, T8, and T12 sites, and a representative structure on a T12 site with ν 1038 cm^{-1} is shown in Figure 10d. The initial geometries for these structures were generated from optimized geometries for Cr dioxo species anchored on double Al-atom sites by changing the Cr structure

DOI: 10.1021/acscatal.5b00333
ACS Catal. 2015, 5, 3078−3092

Table 2. Vibrational Modes (Symmetric Stretch ν_s, Asymmetric Stretch ν_{as}, and Bend δ) of Cr Oxide Species Anchored on Si Sites on the External Surface[a]

(a) Dioxo Cr Species				
	Cr oxidation state	ν_s(O=Cr=O), cm^{-1}	ν_{as}(O=Cr=O), cm^{-1}	δ(O=Cr=O), cm^{-1}
$(Si-O-)_2Cr(=O)_2$ on the external surface	+6	930–939	971–986	310–312
experimental Raman band in Figure 7c		984		
(b) Mono-oxo Cr Species				
		Cr oxidation state		ν(Cr=O), cm^{-1}
$(Si-O-)_4Cr(=O)$ on the external surface		+6		999–1002
experimental Raman band in Figure 7				1017

[a]Results obtained with DFT calculations with DMol^3 using a 64-T cluster zeolite model.

into a mono-oxo and then moving it to one of the Al sites. The configuration shown in Figure 10d with the binding to a framework Al atom through neighboring framework O atoms as O–Al–O is more stable than similar structures bonded simultaneously to Al and Si framework atoms as O–Si–O–Al. For example, the binding to the O–Al–O site in T12 (Figure 10d) is more stable by 32 kJ/mol than that to the O–Si–O–Al site for the Si atom in T11. This preferential binding to O–Al–O framework atoms is in line with the anchoring of the $[Cr(=O)_2OH]^+$ structure shown in Figure 10b. An additional configuration for the $[Cr(=O)]^+$ species was evaluated by bridge-bonding to a pair of Al atoms in T8–T12 positions, similarly to the structures in Figures 10a,c. However, in order to keep the Cr atom in the +3 oxidation state, the Al atom in the T8 site in this case was counterbalanced by an H^+. Such a configuration across a pair of Al sites for $[Cr(=O)]^+$ species was found to be stable but less energetically favorable by 88 kJ/mol than the most stable configuration on a single Al-atom site in Figure 10d. These results suggest that, after reduction of Cr(VI) dioxo species, the formed Cr(III) mono-oxo species are likely to migrate from double to single Al framework anchoring sites. The calculated normal vibrational mode values of 1017–1048 cm^{-1} (Table 1b) for Cr mono-oxo species as $[Cr(=O)]^{2+}$ and $[Cr(=O)]^+$ structures match the position of the experimental Raman band at 1033 cm^{-1} in Figures 7–9.

Silanol Si–O–H groups on the external surface of the zeolite are similar to the silanol groups on the surface of amorphous SiO_2. Our previous computational study evaluated the structure and anchoring sites of Cr oxide species on SiO_2 surfaces and concluded that dioxo $(Si-O-)_2Cr(=O)_2$ species are dominant with some presence of mono-oxo $(Si-O-)_4Cr(=O)$ species.[30] In this study, anchoring of these species on Si sites on the external surface of the zeolite was evaluated by replacing H atoms of terminal OH groups with Cr oxide species and relaxing the positions of the bonding O atoms. Anchoring of dioxo $(Si-O-)_2Cr(=O)_2$ species was evaluated for Si atoms in the following T site pairs: T1–T4, T1–T5, and T9–T9. A representative structure anchored on a pair of Si atoms in T1–T5 sites is shown in Figure 10e. In this structure, the Cr atom is terminated with two O atoms and bonded through two terminal O atoms to two surface Si atoms. The calculated normal vibrational modes ν_s 930–939 cm^{-1} (Table 2a) are close to the position of the experimental Raman band at 984 cm^{-1} in Figure 7c. The zeolite models in this study were designed mainly for examining anchoring sites in the zeolite framework. The agreement between computational and experimental vibrational frequencies for Cr oxide species anchored on framework sites is, therefore, better. The models of the external zeolite surface can be improved by including surface relaxation effects.[32]

The relative stability of Cr dioxo species for anchoring on double Al-atom framework sites (Figure 10a) versus Si sites on the external surface of the zeolite (Figure 10e) was estimated by generating structures with the same stoichiometry. The first structure was generated by relaxing two terminal OH groups for Si sites in the T1 and T5 positions on the edge of the cluster for the configuration in Figure 10a with a Cr dioxo structure bonded to a T8–T12 pair of Al sites. The second structure was generated by replacing the two H atoms of the relaxed OH groups on Si sites in the T1 and T5 positions by a Cr dioxo species and then placing the two replaced H atoms as counterions for the T8 and T12 Al sites. The second structure, which represents anchoring on Si sites on the external surface, is more stable by 79 kJ/mol than the first structure, which represents anchoring on framework Al sites. This result suggests that, under certain conditions, Cr dioxo species may preferentially anchor on Si sites on the external surface of the zeolite.

The mono-oxo $(Si-O-)_4Cr(=O)$ structure binds not to two but to four surface O atoms and has a single terminating O atom. This structure was evaluated for Si atoms on the following anchoring T sites: T1–T5 (bonding through two O atoms for each of the two Si atoms) and 2T9–2T12 (bonding through one O atom for each of the four Si atoms). A representative structure anchored on four Si atoms in T9–T9–T12–T12 sites is shown in Figure 10f. The calculated normal vibrational modes ν 999–1002 cm^{-1} (Table 2b) are close to the position of the experimental Raman band at 1017 cm^{-1} in Figure 7.

Zeolites are known to have vacancy defects caused by missing Al and Si framework atoms. If a Cr atom anchors in such a vacancy defect site and has a single terminating O atom, it generates the same mono-oxo $(Si-O-)_4Cr(=O)$ structure as on the external surface of the zeolite (Figure 10f). A representative Cr mono-oxo structure in a T12 vacancy defect is shown in Figure 10g. Similar structures were obtained for T8 and T11 sites.

Although the structures of Cr mono-oxo species anchored on Si sites on the external surface of the zeolite and in a framework vacancy defect site are similar, their predicted normal vibrational modes are significantly different due to differences in the Cr bonding. The Cr atom in a vacancy site is embedded into the zeolite structure and bonded to Si atoms not through terminal O atoms from surface silanol groups but through framework O atoms. The calculated normal vibrational modes (Table 3) for the mono-oxo $(Si-O-)_4Cr(=O)$ structure in vacancy defect sites ν 926–949 cm^{-1} (for vacancies in T8, T11,

DOI: 10.1021/acscatal.5b00333
ACS Catal. 2015, 5, 3078–3092

Table 3. Vibrational Modes (Stretch ν) of Cr Mono-oxo Species Anchored on Defect Sites due to a Si or Al-Atom Framework Vacancy[a]

	Cr oxidation state	ν(Cr=O), cm^{-1}
$(Si-O-)_4Cr(=O)$ in a vacancy defect without neighboring Al atoms (DMol^3 calculations)	+6	926–949
$(Si-O-)_4Cr(=O)$ in a vacancy defect with one neighboring Al atom (Gaussian 09 calculations)	+6	898–962
$(Si-O-)_4Cr(=O)$ in a vacancy defect with two neighboring Al atoms (Gaussian 09 calculations)	+6	899–967
experimental Raman feature in Figure 7c		~900

[a]Results obtained with DFT calculations with DMol^3 using a 64-T cluster zeolite model and with Gaussian 09 using a 46-T cluster zeolite model.

and T12 sites without Al neighboring atoms, DMol^3), 898–962 cm^{-1} (for vacancies in T8 and T7 sites with one Al neighboring atom in respectively T8 and T10 sites; Gaussian 09, Figure 11c and Figure S3b in the Supporting Information), and 899–967 cm^{-1} (for a vacancy in a T7 site with two Al neighboring atoms in T8–T8 positions; Gaussian 09, Figure 11b) are close to the position of the broad experimental Raman feature at ~900 cm^{-1} in Figure 7c.

4. DISCUSSION

The Si–O–H silanol groups on the external surface of the zeolite are similar to those on the surface of amorphous SiO_2. Therefore, zeolites with a low concentration of Al (high Si/Al ratios) should have anchoring sites and Cr oxide structures that are similar to those on SiO_2 supports. Our previous Raman spectroscopic studies show that dehydrated Cr/SiO_2 catalysts have mainly isolated Cr oxide species (species with a single Cr atom) with Raman bands at 982 and 1011 cm^{-1}.[26−29] The structure of Cr/SiO_2 catalysts has been extensively studied,[1−6] and the dominance of isolated surface Cr species is consistent with multiple characterization studies: for example, with results obtained with extended X-ray absorption fine structure (EXAFS) and X-ray absorption near edge structure (XANES) spectroscopies[45−48] and with characterization of a model $CrO_x/SiO_2/Si(110)$ system with XPS, secondary-ion mass spectrometry (SIMS), and Rutherford backscattering spectrometry (RBS).[49] Our computational study of isolated Cr(VI) oxide species supported on SiO_2 identified two main types of Cr structures: (1) a dioxo $(Si-O-)_2Cr(=O)_2$ structure with a symmetric stretching vibration ν_s for the O=Cr=O fragment that matches the experimental Raman band at 982 cm^{-1} and (2) a mono-oxo $(Si-O-)_4Cr(=O)$ structure with a stretching vibration ν for the Cr=O fragment that matches the experimental Raman band at 1011 cm^{-1}.[30]

The Raman spectrum for the catalyst with 1 wt % Cr supported on the ZSM-5 zeolite with the lowest evaluated Al concentration (highest Si/Al = 140) in Figure 7b exhibits similar bands at 984 and 1017 cm^{-1}. The structures for Cr(VI) dioxo $(Si-O-)_2Cr(=O)_2$ (Figures 10e and 12e) and Cr(VI) mono-oxo $(Si-O-)_4Cr(=O)$ (Figures 10f and 12f) species on Si sites on the external surface of ZSM-5 obtained with DFT calculations are analogous to the same structures on SiO_2 surfaces with similar vibrational frequencies (Table 2). The Raman bands at 984 and 1017 cm^{-1}, therefore, can be respectively assigned to dioxo $(Si-O-)_2Cr(=O)_2$ and mono-oxo $(Si-O-)_4Cr(=O)$ structures on the external surface of ZSM-5 zeolites. Anchoring of Cr oxide species on Si sites on the external surface is consistent with a decrease in the intensity of the Si–O–H silanol vibrations at 3741 cm^{-1} with increasing Cr loading in the IR spectra in Figure 6 and with an increase in the intensity of the UV–vis band at 460 nm for Cr oxide species anchored on Si sites with increasing Si/Al ratio in Figure 5. The increase in the intensity of the Raman band at 1017 cm^{-1} with increasing Cr loading at a constant Si/Al ratio of 15 in Figure 7a, consequently, signifies that Cr oxide species preferentially anchor on Al sites and then, as the number of Al sites per Cr atom decreases, begin to anchor on Si sites on the external surface of the zeolite. This trend is consistent with the changes in the Raman spectra in Figure 7b for catalysts with increasing Si/Al ratios at a constant 1 wt % Cr loading.

The structure of surface Cr oxide species depends not only on the catalyst composition but also on the environment. When the 1 wt % Cr/ZSM-5 (Si/Al = 25, 40, 140) catalyst samples are treated under an O_2 flow at 773 K, their Raman spectra exhibit dominant bands at 984 and 1017 cm^{-1} for respectively dioxo $(Si-O-)_2Cr(=O)_2$ and mono-oxo $(Si-O-)_4Cr(=O)$ structures on the external surface of ZSM-5. These spectra are different from the spectra in Figure 7b obtained under the same O_2 flow but at a lower temperature of 383 K, signifying that an exposure to gas-phase O_2 at elevated temperatures forces a migration of Cr oxide species to the external surface of the zeolite. This effect, however, is not observed for the 0.5 wt % Cr/ZSM-5 (Si/Al = 15) catalyst with a relatively low Cr loading and low Si/Al ratio, as its Raman spectra under the O_2 flow at 773 K shown in Figure 8 do not exhibit bands at 984 and 1017 cm^{-1}. The migration of Cr oxide species to the external surface, therefore, is observed only when there are relatively few Al anchoring sites for each Cr atom. The ease of migration of surface Cr oxide structures for ZSM-5 supports is in line with the reported mobility for Cr oxide species supported on SiO_2, Al_2O_3, and a mordenite zeolite.[44]

A broad Raman feature at ~900 cm^{-1} for 1 wt % Cr/ZSM-5 (Si/Al = 25–140) can be assigned to the mono-oxo $(Si-O-)_4Cr(=O)$ structure in a defect zeolite site caused by a Si or Al-atom vacancy (Figures 10g, 11b,c, and 12g and Figures S3b and S4c in the Supporting Information) on the basis of an agreement with the calculated vibrational frequencies in Table 3. In this structure, the Cr atom is embedded into the zeolite framework, in effect replacing a framework Si or Al atom, which is analogous to the Cr(VI) mono-oxo structure identified for Cr substitution in a beta silicalite.[25] The number of defect sites is expected to be small and, consequently, Cr mono-oxo structures anchored on these sites are observed only as a small minority species. Another small feature at ~1135 cm^{-1} observed in Raman spectra in Figure 7 is possibly due to Cr oxide species anchored on extraframework Al sites, since the fraction of these anchoring sites should also be relatively low and since their surface OH groups with the IR peaks at 3783 and 3660 cm^{-1} in Figure 6 are perturbed after Cr deposition. Furthermore, another small fraction of Cr atoms is present in the form of crystalline Cr_2O_3 nanoparticles. Supported Cr oxide species are likely to increasingly agglomerate into Cr_2O_3 nanoparticles as the number of Al anchoring sites decreases, since this crystalline Cr oxide phase with a broad UV–vis band at ~600 nm in Figure 5 is observed only for the ZSM-5 sample with the lowest evaluated Al concentration (Si/Al = 140). The formation of Cr_2O_3 nanoparticles on the surface of the silica-rich ZSM-5 (Si/Al = 140) zeolite is consistent with the increase in the amount of Cr_2O_3 nanoparticles with increasing Si

DOI: 10.1021/acscatal.5b00333
ACS Catal. 2015, 5, 3078–3092

content and Cr loading observed for $Cr/SiO_2-Al_2O_3$ catalysts.[50]

The majority of Cr oxide species anchor on framework Al sites, as evidenced by the dominant UV−vis bands at 252 and 324 nm in Figure 5. This preferential anchoring on Al sites is consistent with the evaluation of mobility and preferential anchoring of Cr oxide species on SiO_2, Al_2O_3, and mordenite zeolite supports.[44] The major experimental Raman bands at 964 and 1033 cm^{-1} in Figures 7−9 allow identification of the main surface Cr oxide species on the basis of an agreement with the calculated vibrational frequencies in Table 1. The Raman band at 964 cm^{-1} can be assigned to the Cr(VI) dioxo structures anchored on single and double Al-atom framework sites: $[Cr(=O)_2]^{2+}$ on two $[AlO_4]^-$ (Figures 10a, 11a, 12a and Figures S3a and S4a,b in the Supporting Information) and $[Cr(=O)_2OH]^+$ on one $[AlO_4]^-$ (Figures 10b and 12b). The first structure has two bonding framework O atoms and two terminal O atoms, and it can also be represented as the chromate ion $[O-[Cr(=O)_2]-O]^{2+}$, which counterbalances the charge of two framework Al sites. This structure was previously proposed as dominant on the basis of DRS measurements for Cr oxide species supported on several zeolites.[22] In the second structure, the absence of the second anchoring Al atom is compensated by a hydroxyl group, and the Cr atom remains in the +6 oxidation state. At least a fraction of Cr(VI) dioxo species must be in the form of $[Cr(=O)_2OH]^+$ species anchored on single Al-atom framework sites, because the IR spectra in Figure 6 exhibit an increase in the intensity of the band at 3608 cm^{-1} after Cr deposition due to vibrations of OH groups on framework Al sites or on Cr oxide species. As the OH groups on framework Al sites are replaced by anchoring Cr oxide species, their loss must be compensated by the OH groups in the $[Cr(=O)_2OH]^+$ structures.

The Raman band at 1033 cm^{-1} can be assigned to the Cr mono-oxo structures anchored on single and double Al-atom framework sites: $[Cr(=O)]^{2+}$ on two $[AlO_4]^-$ (Figures 10c and 12c) and $[Cr(=O)]^+$ on one $[AlO_4]^-$ (Figures 10d and 12d). The second structure with the Cr atom in the oxidation state of +3 is more likely, since the color of Cr/ZSM-5 samples changes visibly after an Ar purge at 773 K to green, indicative of Cr(III) cations (Figure 3). In contrast, the Cr atom in the first structure has an oxidation state of +4. Since the Cr(IV) oxide is black, the presence of the first structure is less likely. XPS studies of Cr/ZSM-5 catalysts indicate the presence of initial Cr(VI) oxide species that reduce into Cr(III) oxide species under reaction conditions with methane at 1023 K.[24]

In addition to Si−O−H silanol groups on the external surface of the zeolite, ZSM-5 samples may also have defect silanol groups in the zeolite framework. Since our IR spectra in Figure 6 exhibit a single silanol peak at 3741 cm^{-1} for the external surface, and the characteristic peaks at 3700 and 3730 cm^{-1} for defect silanols[51] are not observed, such defect silanols were not included in the analysis of possible anchoring sites. Furthermore, a Cr oxide structure anchored on a framework Al site and a neighboring defect silanol would be similar to a structure on a framework O−Si−O−Al site. Our calculation results show that such an O−Si−O−Al anchoring site is less preferable than bonding directly to an Al framework site on O−Al−O (Figures 10b,d and 12b,d). Therefore, even in the presence of defect silanols, anchoring of Cr oxide species on framework Al sites should not be affected.

The Cr(VI) dioxo structures $[Cr(=O)_2]^{2+}$ anchored on two $[AlO_4]^-$ sites and $[Cr(=O)_2OH]^+$ anchored on one $[AlO_4]^-$ site autoreduce under an Ar flow at 773 K, as evidenced by the disappearance of their characteristic Raman band at 964 cm^{-1} in Figure 8. The Cr(III) mono-oxo $[Cr(=O)]^+$ structure on one $[AlO_4]^-$ site is stable under these conditions. Furthermore, only this Cr(III) mono-oxo structure is observed in the Raman spectrum in Figure 9a for Cr/ZSM-5 under similar conditions prior to reaction with methane. The observed autoreduction of Cr(VI) dioxo structures on Al framework anchoring sites at 773 K is consistent with the reported lower temperatures for reduction under an H_2 flow at ∼560 K for bulk CrO_3 and at ∼570 K for Cr/ZSM-5[15] and with reduction of Cr(VI) to Cr(III) for $Cr/SiO_2-Al_2O_3$ monitored with UV−vis DRS measurements under reaction conditions with *n*-butane at 773 K.[52] The stability of the Cr(III) mono-oxo structure is also consistent with the stability of Cr(III) oxide species against recalcination at 823 K reported for $Cr/SiO_2-Al_2O_3$ and Cr/Al_2O_3 catalysts.[43] The ratio of Cr(III) oxide species for $Cr/SiO_2-Al_2O_3$ catalysts was found to increase with increasing Al content of the support, Cr loading, and reduction temperature.[43]

The identification of Cr oxide structures and their anchoring sites provides a starting point for an analysis of reaction testing results. The reaction testing results in Figure 4 show that the 0.8 wt % Cr/ZSM-5 (Si/Al = 15) catalyst is significantly less active in methane dehydroaromatization than the 1.5 wt % Mo/ZSM-5 (Si/Al = 15) catalyst. Both catalysts have the same metal loading: moles of Cr or Mo per gram of ZSM-5. The low rate of benzene formation for the Cr catalyst, however, is relatively stable, whereas it declines rapidly with time on stream for the Mo catalyst. Initial Mo oxide structures are known to reduce and agglomerate into Mo carbide or oxycarbide nanoparticles.[32] A decline in the activity of Mo/ZSM-5 catalysts is usually attributed to both agglomeration of Mo species and accumulation of carbonaceous deposits on the surface of carbided Mo nanoparticles as well as in zeolite pores. In contrast with Mo/ZSM-5 catalysts, previously reported XPS measurements for a 2 wt % Cr/ZSM-5 (Si/Al = 25) catalyst suggest that initial Cr(VI) oxide species are only partially reduced under reaction with methane and convert into Cr(III) oxide structures that remain catalytically active during methane dehydroaromatization at 1023 K.[24] The disappearance of the band at 1033 cm^{-1} for Cr(III) mono-oxo species $[Cr(=O)]^+$ anchored on framework $[AlO_4]^-$ sites (Figures 10d and 12d) in the operando Raman spectra in Figure 9a collected under reaction conditions with methane, therefore, suggests not a complete reduction and carburization of Cr oxide species but accumulation of carbonaceous deposits with a Raman band at 1062 cm^{-1} on the surface of catalytically active Cr(III) oxide species. The activity of Cr(III) oxide species is evidenced by the MS measurements in Figures 3 and 9b that exhibit immediate detection of benzene and hydrogen as reaction products after methane introduction.

When the Cr loading is doubled from 0.8 to 1.6 wt % for ZSM-5 (Si/Al = 15), the benzene and hydrogen formation rates per Cr atom decline by a factor of about 2 (Figure S2 in the Supporting Information). On the other hand, the Raman spectra in Figure 7a demonstrate that the distribution of initial Cr oxide species for Cr loadings from 0.5 to 2.6 wt % stays substantially the same with the main Raman bands at 964 cm^{-1} for Cr dioxo species (Table 1a) and at 1033 cm^{-1} for Cr mono-oxo species (Table 1b) anchored on framework Al sites. Only a fraction of the Cr mono-oxo species anchors on Si sites on the external surface of the zeolite at 1.6 wt % Cr (Raman band at

DOI: 10.1021/acscatal.5b00333
ACS Catal. 2015, 5, 3078−3092

1017 cm^{-1} in Figure 7a and calculated frequencies in Table 2b). Even if the activity of Cr species on Si anchoring sites is significantly lower than that of Cr species anchored on Al sites, such a difference cannot account for the decrease in activity with increasing Cr loading from 0.8 and 1.6 wt %. Therefore, the initial Cr oxide species must be transforming under reaction conditions. Initial isolated Cr structures likely agglomerate into clusters and nanoparticles, as previously suggested on the basis of ESR and XPS measurements,[24] with the extent of agglomeration increasing with the Cr loading. It is also possible that the lower Cr/Al ratio at higher Cr loadings forces a migration of Cr species under reaction conditions from framework Al sites to Si sites on the external surface of the zeolite where the Cr species become less active, similarly to the observed migration from Al to Si sites for 1 wt % Cr/ZSM-5 catalysts in the presence of gas-phase O_2 when the temperature is increased from 383 to 773 K for ZSM-5 supports with Si/Al ratios greater than 25 (Figure 7b,c).

The similarity in reaction rates for 0.8 wt % Cr/ZSM-5 (Si/Al = 15) catalysts prepared by impregnation and as a 1:1 physical mixture of 1.6 wt % Cr/ZSM-5 (Si/Al = 15) and the blank ZSM-5 (Si/Al = 15) zeolite in Figure 4 demonstrates that Cr species are highly mobile and can migrate from the impregnated part of the catalyst to the particles of the blank ZSM-5. Such a migration provides additional anchoring sites for Cr species and, therefore, limits their agglomeration and maintains their catalytic activity. The Cr loading, therefore, must have an optimal value for increasing the catalytic performance. The Cr loading of 2 wt % was previously reported as optimal for ZSM-5 (Si/Al = 25) after catalyst calcination at 773 K for 5 h.[23] Longer durations of the calcination pretreatment (the current study employed 1 h) are likely to force agglomeration of the Cr oxide phase and, thus, shift the optimal Cr loadings to higher values. An additional factor in catalyst performance optimization is the dual role of framework Al sites. Cr/ZSM-5 catalysts are likely bifunctional with Cr and framework Al active sites. The Cr sites activate methane and likely form C_2 hydrocarbon intermediates, which then react on framework Al acid sites and form aromatic hydrocarbons. The framework Al sites, therefore, serve as anchoring sites for Cr species as well as active sites for hydrocarbon reactions. The importance of zeolite acid sites at a constant 2 wt % Cr loading was demonstrated by adjusting the Na^+/H^+ ratio for ZSM-5 (Si/Al = 25): both the methane conversion and benzene selectivity increased with increasing acidity.[23] Despite these insights, transformations of Cr species and their interactions with acid sites under reaction conditions remain largely unknown and require additional studies. For example, the reported effect of a pretreatment with CO, which increases benzene formation rates and selectivities,[23] remains unexplained.

Molecular structures of zeolite-supported Cr oxide species reported in this study (Figures 10–12 and Figures S3 and S4 in the Supporting Information) were obtained with DFT calculations using three different codes: DMol[3], Gaussian 09, and VASP. Calculations with different computational methods provide a cross-check of the results. Incorporation of framework relaxation effects around framework Al sites and anchored Cr oxide species required use of relatively large clusters: a 64-T cluster for DMol[3] (Figure 1) and two separate 46-T clusters for Gaussian 09 calculations (Figure 2 and Figure S1 in the Supporting Information). An additional advantage of clusters of this size is the ability to use a single model for evaluating multiple framework sites for anchoring of Cr oxide species away from the constrained cluster edges. An agreement between the results obtained with DMol[3] and Gaussian 09 cluster calculations confirms the structures of Cr oxide species. An agreement between the results obtained with the cluster calculations and with the periodic VASP calculations using the full ZSM-5 unit cell provides an additional confirmation for the results and, furthermore, verification of the selection of cluster sizes and edge constraints. Although the molecular structures obtained with the different DFT codes are similar, their predicted normal vibrational modes had to be scaled with a different scaling factor for each combination of the DFT method and basis set. After the scaling, the adjusted vibrational modes from the three DFT codes were substantially similar (Tables 1 and 3).

The current investigation on the nature of zeolite-supported Cr oxide structures and their anchoring sites provides an example of close integration between experimental and computational studies. Initial DFT models were constructed on the basis of catalyst characterization with in situ UV–vis and IR spectroscopies (Figures 5 and 6). A comparison between normal vibrational modes calculated with the initial DFT models and experimental Raman bands in Figure 7a allowed identification of some Cr oxide structures and led to the development of additional models. Since the calculations predict a relatively broad range of vibrational frequencies for some types of Cr oxide structures depending on the T-site positions of their anchoring sites and since there is usually a general but not perfect agreement between calculated and experimental vibrational frequencies, further experimental measurements were performed for additional catalyst formulations (Figure 7b) and under additional conditions (Figures 3b, 7c, and 8) in order to verify computational assignments. The additional experimental results were then used to improve and refine computational models. In summary, our integrated experimental–computational methodology uses iterative cycles where experimental results guide model development and then modeling results guide the selection of additional experiments, which in turn guide model improvements. The identified Cr oxide structures and their anchoring sites provide a consistent interpretation for all of our experimental characterization measurements and a starting point for analyzing reaction testing results. The results will be helpful in developing improved catalysts for methane dehydroaromatization, for developing structure–activity relations for Cr/ZSM-5 catalysts in multiple other applications, and for identifying Cr oxide structures on other zeolite supports as well as for identifying oxide structures of other transition metals on ZSM-5 and other zeolites.

5. CONCLUSIONS

The structure and anchoring sites of Cr oxide species supported on ZSM-5 zeolites were identified with a closely integrated experimental and computational study. Two sets of Cr/ZSM-5 catalysts were evaluated. In the first set, the Cr loading was varied from 0.5 to 2.6 wt % using the same H-ZSM-5 (Si/Al = 15) support. In the second set, the Si/Al ratio of the H-ZSM-5 support was varied from 15 to 140 using a constant 1 wt % Cr loading. The catalysts were characterized with in situ UV–vis, IR, and Raman spectroscopies, including operando Raman measurements under reaction conditions with methane at 773–1123 K with simultaneous MS analysis of reaction products. DFT calculations with cluster zeolite models were performed

DOI: 10.1021/acscatal.5b00333
ACS Catal. 2015, 5, 3078–3092

with the DMol^3 code in Materials Studio software and with Gaussian 09 software. In addition, periodic DFT calculations with the full ZSM-5 unit cell were performed with the VASP code.

Isolated Cr(VI) dioxo and Cr(III) mono-oxo structures (structures with a single Cr atom) on framework Al anchoring sites were identified as the dominant species in the presence of gas-phase O_2 under most conditions (UV−vis bands at 252, 324, and 460 nm, Raman bands at 964 and 1033 cm^{-1}). The Cr(III) mono-oxo species anchor on single framework Al-atom sites as a $[Cr(=O)]^+$ structure (characteristic Raman band at 1033 cm^{-1}). The Cr(VI) dioxo species may anchor on single or double framework Al-atom sites. A double Al-atom site is composed of two Al atoms that are sufficiently close in the zeolite framework in order to bridge-bond an isolated Cr oxide structure. The Cr(VI) dioxo species anchor on single Al-atom sites as a $[Cr(=O)_2OH]^+$ structure. On double Al-atom sites, the Cr(VI) dioxo species anchor as a $[Cr(=O)_2]^{2+}$ structure. Both of these Cr(VI) dioxo structures have the same characteristic Raman band at 964 cm^{-1}.

In the absence of gas-phase O_2 (under Ar flow) at 773 K, the Cr(VI) dioxo species on framework Al anchoring sites autoreduce, and their characteristic Raman band at 964 cm^{-1} is not observed. The Cr(III) mono-oxo species with their characteristic Raman band at 1033 cm^{-1} remain the only observable Cr oxide structures under these conditions.

For ZSM-5 zeolites with a relatively low concentration of framework Al atoms (Si/Al ≥ 25), exposure to gas-phase O_2 at 773 K forces Cr oxide species to migrate from framework Al anchoring sites to Si sites on the external surface of the zeolite. The Raman spectra for Cr/ZSM-5 catalysts under these conditions exhibit dominant bands at 984 cm^{-1} for Cr(VI) dioxo species as a $(Si-O-)_2Cr(=O)_2$ structure and at 1017 cm^{-1} for Cr(VI) mono-oxo species as a $(Si-O-)_4Cr(=O)$ structure. These isolated Cr oxide structures and their Raman bands are similar to those reported previously for Cr/SiO_2 catalysts.

In addition to the dominant isolated Cr oxide structures anchored on framework Al sites and Si sites on the external surface of the zeolite, a fraction of Cr atoms anchors in zeolite vacancy defect sites and on extraframework Al sites. Formation of some crystalline Cr_2O_3 nanoparticles is also detected.

Cr/ZSM-5 catalysts are active in methane dehydroaromatization. The catalytic activity of Cr/ZSM-5 catalysts is significantly lower than that of Mo/ZSM-5 catalysts. The rate of benzene formation over Cr/ZSM-5 catalysts, however, is relatively stable with time on stream in comparison to a rapidly declining rate over Mo/ZSM-5 catalysts. Initial Cr oxide species are immediately active in benzene and hydrogen formation. The Cr species under reaction conditions are highly mobile and can migrate not only on the zeolite surface but also between zeolite particles. This ease of migration is evidenced by the similarity in catalytic performance for 0.8 wt % Cr/ZSM-5 (Si/Al = 15) catalysts prepared by impregnation and by physically mixing 1.6 wt % Cr/ZSM-5 (Si/Al = 15) and ZSM-5 (Si/Al = 15).

The identification of Cr oxide structures and their anchoring sites on ZSM-5 zeolites will be helpful in the development of improved zeolite-supported catalysts where Cr serves as the main component or as a promoter and in the identification of oxide structures of other transition metals on ZSM-5 and other zeolite types.

■ ASSOCIATED CONTENT

Supporting Information

The following file is available free of charge on the ACS Publications website at DOI: 10.1021/acscatal.5b00333.

An additional 46-T cluster model of the ZSM-5 zeolite structure, reaction rates for 0.8 and 1.6 wt % Cr/ZSM-5 (Si/Al = 15) catalysts in catalytic methane dehydroaromatization, and additional optimized structures obtained with Gaussian 09 and VASP DFT calculations (PDF)

■ AUTHOR INFORMATION

Corresponding Authors

*E-mail for R.G.: ncgrybos@cyf-kr.edu.pl.
*E-mail for J.H.: jhandz@pk.edu.pl.
*E-mail for I.E.W.: iew0@lehigh.edu.
*E-mail for S.G.P.: Simon.Podkolzin@Stevens.edu.

Notes

The authors declare no competing financial interest.

■ ACKNOWLEDGMENTS

The work in the I.E.W. group at Lehigh University was supported by National Science Foundation Grant CBET-1134012. The work in the S.G.P. group at the Stevens Institute of Technology was supported by National Science Foundation Grant CBET-1133987. The DFT calculations in the S.G.P. group were performed with Materials Studio program, provided by BIOVIA Corp. under a collaborative research license. We thank Dr. Jason de Joannis at BIOVIA Corp. for discussions on computational parameters. We thank PQ Corp. for providing ZSM-5 zeolite samples and Dr. Istvan Halasz at PQ Corp. for discussions on zeolite characterization. J.H. acknowledges financial support from the Polish National Science Centre (Project No. N N204 131039, 2010−2012) and the computing resources from PL-Grid Infrastructure and Academic Computer Centre CYFRONET AGH (grants MNiSW/IBM_BC_HS21/PK/044/2007 and MNiSW/IBM_BC_HS21/PK/003/2013).

■ REFERENCES

(1) Weckhuysen, B. M.; Wachs, I. E.; Schoonheydt, R. A. *Chem. Rev.* **1996**, *96*, 3327−3349.
(2) Weckhuysen, B. M.; Schoonheydt, R. A. *Catal. Today* **1999**, *51*, 215−221.
(3) Beck, J. S.; Haag, W. O.; Buonomo, F.; Sanfilippo, D.; Trifirò, F.; Arnold, H.; Döbert, F.; Gaube, J. In *Handbook of Heterogeneous Catalysis*; Ertl, G., Knözinger, H., Weitkamp, J., Eds.; Wiley-VCH: Weinheim, Germany, 2008; Organic Reactions, Sections 4.1−4.4, pp 2123−2231.
(4) McDaniel, M. P. A Review of the Phillips Supported Chromium Catalyst and Its Commercial Use for Ethylene Polymerization. In *Advances in Catalysis*; Gates, B. C., Knözinger, H., Eds.; Academic Press: San Diego, CA, 2010; Vol. *53*, Chapter 3, pp 123−606.
(5) Weckhuysen, B. M.; Schoonheydt, R. A. *Catal. Today* **1999**, *51*, 223−232.
(6) Bhasin, M. M.; McCain, J. H.; Vora, B. V.; Imai, T.; Pujadó, P. R. *Appl. Catal., A* **2001**, *221*, 397−419.
(7) Chaudhari, P. K.; Saini, P. K.; Chand, S. *J. Sci. Ind. Res.* **2002**, *61*, 810−816.
(8) Abdullah, A. Z.; Bakar, M. Z.; Bhatia, S. *Ind. Eng. Chem. Res.* **2003**, *42*, 5737−5744.
(9) Swanson, M. E.; Greene, H. L.; Qutubuddin, S. *Appl. Catal., B* **2004**, *52*, 91−108.
(10) Rachapudi, R.; Chintawar, P. S.; Greene, H. L. *J. Catal.* **1999**, *185*, 58−72.

DOI: 10.1021/acscatal.5b00333
ACS Catal. 2015, 5, 3078−3092

(11) Ayari, F.; Mhamdi, M.; Álvarez-Rodríguez, J.; Ruiz, A. R. G.; Delahay, G.; Ghorbel, A. *Appl. Catal., B* **2013**, *134*−*135*, 367−380.
(12) Salker, A. V.; Weisweiler, W. *Appl. Catal., A* **2000**, *203*, 221−229.
(13) Saux, C.; Pierella, L. B. *Appl. Catal., A* **2011**, *400*, 117−121.
(14) Yamashita, H.; Ohshiro, S.; Kida, K.; Yoshizawa, K.; Anpo, M. *Res. Chem. Intermed.* **2003**, *29*, 881−890.
(15) Ayari, F.; Mhamdi, M.; Álvarez-Rodríguez, J.; Guerrero Ruiz, A. R.; Delahay, G.; Ghorbel, A. *Appl. Catal., A* **2012**, *415*−*416*, 132−140.
(16) Ayari, F.; Mhamdi, M.; Debecker, D. P.; Gaigneaux, E. M.; Alvarez-Rodriguez, J.; Guerrero-Ruiz, A.; Delahay, G.; Ghorbel, A. *J. Mol. Catal. A: Chem.* **2011**, *339*, 8−16.
(17) Mimura, N.; Takahara, I.; Inaba, M.; Okamoto, M.; Murata, K. *Catal. Commun.* **2002**, *3*, 257−262.
(18) Dong, Q.; Zhao, X.; Wang, J.; Ichikawa, M. *J. Nat. Gas Chem.* **2004**, *13*, 36−40.
(19) Ereña, J.; Arandes, J. M.; Bilbao, J.; Aguayo, A. T.; De Lasa, H. I. *Ind. Eng. Chem. Res.* **1998**, *37*, 1211−1219.
(20) Mohanty, P.; Majhi, S.; Sahu, J. N.; Pant, K. K. *Ind. Eng. Chem. Res.* **2012**, *51*, 4843−4853.
(21) Yu, Q.; Richter, M.; Li, L.; Kong, F.; Wu, G.; Guan, N. *Catal. Commun.* **2010**, *11*, 955−959.
(22) Weckhuysen, B. M.; Spooren, H. J.; Schoonheydt, R. A. *Zeolites* **1994**, *14*, 450−457.
(23) Weckhuysen, B. M.; Wang, D.; Rosynek, M. P.; Lunsford, J. H. *J. Catal.* **1998**, *175*, 338−346.
(24) Weckhuysen, B. M.; Wang, D.; Rosynek, M. P.; Lunsford, J. H. *J. Catal.* **1998**, *175*, 347−351.
(25) Tielens, F.; Islam, M. M.; Skara, G.; De Proft, F.; Shishido, T.; Dzwigaj, S. *Microporous Mesoporous Mater.* **2012**, *159*, 66−73.
(26) Lee, E. L.; Wachs, I. E. *J. Phys. Chem. C* **2007**, *111*, 14410−14425.
(27) Lee, E. L.; Wachs, I. E. *J. Phys. Chem. C* **2008**, *112*, 6487−6498.
(28) Lee, E. L.; Wachs, I. E. *J. Catal.* **2008**, *258*, 103−110.
(29) Lee, E. L.; Wachs, I. E. *J. Phys. Chem. C* **2008**, *112*, 20418−20428.
(30) Handzlik, J.; Grybos, R.; Tielens, F. *J. Phys. Chem. C* **2013**, *117*, 8138−8149.
(31) Handzlik, J.; Kurleto, K. *Chem. Phys. Lett.* **2013**, *561*−*562*, 87−91.
(32) Gao, J.; Zheng, Y.; Fitzgerald, G. B.; de Joannis, J.; Tang, Y.; Wachs, I. E.; Podkolzin, S. G. *J. Phys. Chem. C* **2014**, *118*, 4670−4679.
(33) Perdew, J. P.; Chevary, J. A.; Vosko, S. H.; Jackson, K. A.; Pederson, M. R.; Singh, D. J.; Fiolhais, C. *Phys. Rev. B: Condens. Matter Mater. Phys.* **1992**, *46*, 6671−6687.
(34) Kresse, G.; Hafner, J. *Phys. Rev. B: Condens. Matter Mater. Phys.* **1993**, *47*, 558−561.
(35) Kresse, G.; Hafner, J. *Phys. Rev. B: Condens. Matter Mater. Phys.* **1994**, *49*, 14251−14269.
(36) Kresse, G.; Joubert, D. *Phys. Rev. B: Condens. Matter Mater. Phys.* **1999**, *59*, 1758−1775.
(37) Olson, D. H.; Kokotailo, G. T.; Lawton, S. L.; Meier, W. M. *J. Phys. Chem.* **1981**, *85*, 2238−2243.
(38) Hope, E. G.; Jones, P. J.; Levason, W.; Ogden, J. S.; Tajik, M.; Turff, J. W. *J. Chem. Soc., Dalton Trans.* **1985**, 529−533.
(39) Hobbs, W. E. *J. Chem. Phys.* **1958**, *28*, 1220−1222.
(40) Wang, X.; Andrews, L. *J. Phys. Chem. A* **2006**, *110*, 10409−10418.
(41) Weigend, F.; Ahlrichs, R. *Phys. Chem. Chem. Phys.* **2005**, *7*, 3297−3305.
(42) Frisch, M. J.; Trucks, G. W.; Schlegel, H. B.; Scuseria, G. E.; Robb, M. A.; Cheeseman, J. R.; Scalmani, G.; Barone, V.; Mennucci, B.; Petersson, G. A.; Nakatsuji, H.; Caricato, M.; Li, X.; Hratchian, H. P.; Izmaylov, A. F.; Bloino, J.; Zheng, G.; Sonnenberg, J. L.; Hada, M.; Ehara, M.; Toyota, K.; Fukuda, R.; Hasegawa, J.; Ishida, M.; Nakajima, T.; Honda, Y.; Kitao, O.; Nakai, H.; Vreven, T.; Montgomery, J. A., Jr.; Peralta, J. E.; Ogliaro, F.; Bearpark, M.; Heyd, J. J.; Brothers, E.; Kudin, K. N.; Staroverov, V. N.; Kobayashi, R.; Normand, J.; Raghavachari, K.; Rendell, A.; Burant, J. C.; Iyengar, S. S.; Tomasi, J.; Cossi, M.; Rega, N.; Millam, J. M.; Klene, M.; Knox, J. E.; Cross, J. B.; Bakken, V.; Adamo, C.; Jaramillo, J.; Gomperts, R.; Stratmann, R. E.; Yazyev, O.; Austin, A. J.; Cammi, R.; Pomelli, C.; Ochterski, J. W.; Martin, R. L.; Morokuma, K.; Zakrzewski, V. G.; Voth, G. A.; Salvador, P.; Dannenberg, J. J.; Dapprich, S.; Daniels, A. D.; Farkas, Ö.; Foresman, J. B.; Ortiz, J. V.; Cioslowski, J.; Fox, D. J. *Gaussian 09, Revision C.01*; Gaussian, Inc., Wallingford, CT, 2009.
(43) Weckhuysen, B. M.; De Ridder, L. M.; Grobet, P. J.; Schoonheydt, R. A. *J. Phys. Chem.* **1995**, *99*, 320−326.
(44) Weckhuysen, B. M.; Schoofs, B.; Schoonheydt, R. A. *J. Chem. Soc., Faraday Trans.* **1997**, *93*, 2117−2120.
(45) Groppo, E.; Prestipino, C.; Cesano, F.; Bonino, F.; Bordiga, S.; Lamberti, C.; Thüne, P. C.; Niemantsverdriet, J. W.; Zecchina, A. *J. Catal.* **2005**, *230*, 98−108.
(46) Groppo, E.; Lamberti, C.; Bordiga, S.; Spoto, G.; Zecchina, A. *Chem. Rev.* **2005**, *105*, 115−184.
(47) Demmelmaier, C. A.; White, R. E.; van Bokhoven, J. A.; Scott, S. L. *J. Catal.* **2009**, *262*, 44−56.
(48) Moisii, C.; Deguns, E. W.; Lita, A.; Callahan, S. D.; van de Burgt, L. J.; Magana, D.; Stiegman, A. E. *Chem. Mater.* **2006**, *18*, 3965−3975.
(49) Thüne, P. C.; Linke, R.; van Gennip, W. J. H.; de Jong, A. M.; Niemantsverdriet, J. W. *J. Phys. Chem. B* **2001**, *105*, 3073−3078.
(50) Weckhuysen, B. M.; Schoonheydt, R. A.; Jehng, J. M.; Wachs, I. E.; Cho, S. J.; Ryoo, R.; Kijlstra, S.; Poels, E. *J. Chem. Soc., Faraday Trans.* **1995**, *91*, 3245−3253.
(51) Hoffmann, P.; Lobo, J. A. *Microporous Mesoporous Mater.* **2007**, *106*, 122−128.
(52) Weckhuysen, B. M.; Bensalem, A.; Schoonheydt, R. A. *J. Chem. Soc., Faraday Trans.* **1998**, *94*, 2011−2014.

DOI: 10.1021/acscatal.5b00333
ACS Catal. 2015, 5, 3078−3092